WILEY | Hindawi

Research Article

A New Fast and Efficient MPPT Algorithm for Partially Shaded PV Systems Using a Hyperbolic Slime Mould Algorithm

Hamza Belmadani,[1] Rafik Bradai,[2] Aissa Kheldoun,[3] Karam Khairullah Mohammed [ID],[4] Saad Mekhilef [ID],[5] Youcef Belkhier [ID],[6] and Adel Oubelaid [ID][7]

[1]*SET Laboratory, Faculty of Technology, Electronics Department, Blida 1 University, 09000 Blida, Algeria*
[2]*LATSI, Faculty of Technology, Electronics Department, Blida 1 University, 09000 Blida, Algeria*
[3]*Laboratory of Signals & Systems, Institute of Electrical and Electronic Engineering, University M'hamed Bougara, Boumerdes 35000, Algeria*
[4]*Department of Electrical Engineering, College of Engineering, University of Mosul, Mosul, Ninawa 41001, Iraq*
[5]*School of Science, Computing and Engineering Technologies, Swinburne University of Technology, Hawthorn, VIC 3122, Australia*
[6]*Institut de Recherche de l'Ecole Navale (EA 3634, IRENav), French Naval Academy, 29240 Brest, France*
[7]*Laboratoire de Technologie Industrielle et de l'Information, Faculté de Technologie, Université de Bejaia, Bejaia 06000, Algeria*

Correspondence should be addressed to Youcef Belkhier; youcef.belkhier@ecole-navale.fr

The design of new efficient maximum power point tracking (MPPT) techniques has become extremely important due to the rapid expansion of photovoltaic (PV) systems. Because under shading conditions the characteristics of PV devices become multimodal having several power peaks, traditional MPPT techniques provide crappy performance. In turn, metaheuristic algorithms have become massively employed as a typical substitute in maximum power point tracking. In this work, a new optimizer, which was named the hyperbolic slime mould algorithm (HSMA), is designed to be employed as an efficient MPPT algorithm. The hyperbolic tangent function is incorporated into the optimizer framework equations to scale down large perturbations in the tracking stage and boost its convergence trend. Moreover, to provide a strong exploration capability, a new mechanism has been developed in such a way the search process is carried out inside the best two power peak regions along the initial iterations. This region inspection mechanism is the prime hallmark of the designed optimizer in avoiding local power peaks and excessive global search operations. The developed algorithm was examined through diverse complicated partial shading conditions to challenge its global and local search abilities. A comparative analysis was carried out against the well-regarded PSO, GWO, and the standard slime mould algorithm. In overall, the designed optimizer defeated its contenders in all aspects offering higher efficiency, superior robustness, faster convergence, and fewer fluctuations to the operating point. An experimental setup that consists of the DSpace microcontroller and a PV emulator was employed to validate the algorithm overall performance. The recorded outcomes outline that the developed optimizer can achieve a tracking time of 0.6 seconds and 0.86 seconds on average, with 99.85% average efficiency under complex partial shading conditions.

1. Introduction

The growing concerns about climate degeneration and the depletion of traditional energy resources have awakened governments to foster the development of renewable energy sources, especially photovoltaic (PV) systems. This energy transition is also driven by the substantial decline of PV technologies' costs and their ease of installation. However, besides the low efficiency of PV devices, their generated power is strongly dependent on the incoming solar irradiance and temperature. This influence can be visualized using power-voltage curves and current-voltage curves. At a certain uniform illuminance level, the generated PV curve is hill-shaped, characterized by a unique top associated with

the PV generator's maximum power point (MPP). In effect, the PV system needs to operate at this point to maximize its efficiency and reduce power losses. However, when a load is directly coupled to the PV generator, the operating point is dictated by the intersection of the load line and the IV characteristic curve. In practice, the resultant operating point is hardly the MPP level, leading to a substantial reduction in the system overall efficiency. To resolve this issue, DC-DC converters are employed as an interface between the PV generator and the system's load side, allowing the impedance seen by the PV device to be changeable. In turn, by properly adjusting the duty cycle of the DC-DC converter, the operating point can be varied accordingly so that it coincides with the MPP level of the PV array. For these reasons, maximum power point tracking (MPPT) algorithms are incorporated into PV systems to monitor the operating point and keep the power as high as possible under any conditions. Undeniably, conventional MPPT techniques like the perturb and observe (P&O) [1] and the incremental conductance (InC) [2, 3] are the most widely investigated and employed [4]. Broadly speaking, these classical approaches are generally grounded on the hill-climbing concept, which is based on perturbing the system along the direction of increasing power. However, one of the major defects of these algorithms is the appearance of oscillations around the MPP level and their inability to handle partial shading conditions. During such circumstances, the shaded cells are impelled to operate in the reverse bias mode leading to the hot spot phenomenon, which causes severe damage to the PV device. At that time, bypass diodes are inserted in parallel with PV modules to provide an alternative path to the current, eliminating the hot spot problem. In effect, although equipping PV modules with bypass diodes affords protection to them, their presence leads to the distortion of the PV and IV characteristics under nonuniform irradiance conditions [5]. The distortion is in the format of multiple peaks occurring in the characteristic curves due to the mismatch conditions. The peak with the largest power level corresponds the global MPP, while the remaining peaks are local MPPs with lower power levels. Because the PV characteristics turn into multimodal curves under PSCs, the task of maximum power point tracking becomes even more challenging and classical MPPT techniques often fail to handle such cases. With their basic structure, they cannot traverse the different regions of the PV characteristics and often get stagnated at one of the local peaks. At that time, metaheuristic algorithms have become a typical substitute due to their stochastic gradient-free foundation and population-based nature. Because they treat problems as black boxes, neither input data nor training is required to lay out the system [6]. Accordingly, with metaheuristic algorithms, maximum power point tracking is treated as an optimization problem, with the power being the objective function controlled through the duty cycle as the decision variable. During the tracking stage, metaheuristic algorithms usually divide the search mechanisms into two main phases: exploration and exploitation. The exploration process is devoted to generate distant solutions to scout as many optimum regions in the search space as possible. The exploitation process on the other hand intends to

inspect the best-discovered region until eventually converging to the global optimum solution. Despite the well-performing global search abilities of metaheuristic algorithms, their behavior and outcomes are largely dictated by their tuned parameters [7]. More often, applying the algorithm as it was designed in its original version might lead to large perturbations during the tracking stage, slow convergence, and eventually poor accuracy. To enhance their tracking performance, modifications are usually necessary to incorporate into their canonical versions. There have been a myriad number of proposed metaheuristic algorithms applied for MPPT among which the particle swarm optimization (PSO) [8–10], grey wolf optimizer (GWO) [11, 12], salp swarm algorithm (SSA) [13, 14], artificial bee colony algorithm (ABC) [15], ant colony optimization (ACO) [16], and flower pollination algorithm [17] were widely employed. Due to its simple structure, the PSO algorithm has been extensively applied in literature along with incorporated amendments. Despite its successful global optimal tracking under partial shading conditions, it exhibits several issues during optimization. The search behavior generates large perturbations of duty cycles due to the velocity term, which is influenced by the inertia ω and the cognitive and social constants. Although reducing these factors might reduce the velocity levels, the algorithm's exploration stage might be negatively affected, leading to local optima stagnation. For instance, in [18], an accelerated PSO version was developed by removing the personal best term form the velocity equation to boost its convergence trend. In other relevant works as in [19], the modifications involve adjusting the PSO parameters making them either increasing or decreasing over the lapse of iterations. In [20], an enhanced autonomous group PSO algorithm was designed by updating the cognitive constants using a combination of cubic and root functions, leading to a better balance between exploration and exploitation. Moreover, the inverse tangent function was inserted into the velocity term to reduce the highly random nature of the algorithm. Accordingly, the results of the algorithm were superior to those of other PSO variants. In [21], the authors introduced a mechanism by which the duty cycles are effectively distributed within the search space to roughly recognize the global optimum region. Once the particles were scattered, the PSO algorithm takes the lead to carry on the tracking process. Even though improvements were observed with the different PSO variants, the conducted experiments in most of the reported works were missing complicated partial shading patterns in which the number of peaks is high and the global MPP is close to the nearest local peak [22]. In such cases, the probability of local optima stagnation is very high and poses a challenging process to the performance of the given algorithm. In other works, the combination of two or more metaheuristic algorithms turned out to be beneficial. These hybrid schemes intend to take advantage of the merits of each algorithm in the exploration and exploitation phases. Some works divide the tracking process by assigning the first iterations to a certain optimizer due to its performant global search and designating the other one to carry on the tracking process along the remaining iterations due

to its good local search operation. For instance, the authors in [23] designed a two-stage MPPT controller that combines an improved version of the artificial bee colony algorithm and the simultaneous heat transfer search algorithm. The first algorithm was appointed to roughly find the global MPP region in the early stages, while the second algorithm took the lead of digging around that region in the remaining stages. Several other techniques split the duty ratios between two algorithms so that the framework equations of one algorithm update a portion of the solutions and the other portion is updated by the mechanisms of the second algorithm. The latter idea was effectively examined in [24] by combining differential evolution and the whale optimization algorithm resulting in a remarkable faster convergence. In [25], the authors merged the grey wolf optimizer for its good exploration capabilities with the Nelder-Mead (NM) technique for its performant local search operation. The resulting hybrid scheme is constructed in such a way a portion of the candidate solutions are updated by the GWO algorithm and then passed to the NM technique undergoing its four fundamental operations. This passage between the GWO algorithm and the NM technique avoided repeated exploration of the search space, leading to a faster convergence trend as reported in the outcomes. Another interesting scheme was designed in [26] by integrating a detection method to distinguish between partial shading conditions and uniform irradiance conditions (UICs) to avoid unnecessary exploration. Moreover, by checking some inequalities on the PV voltage and the PV current, a skipping method was incorporated to eliminate some regions of the search space and perform the tracking process only on a reduced interval. Once the conditions are checked, the snake optimizer (SO) performs the search process on the specified search space with a rapid convergence trend. Despite the observed satisfactory performance, most of the designed MPPT algorithms were benchmarked on partial shading conditions that involve few peaks, which are not quite difficult to handle [27–33]. Moreover, one can observe from their framework equations that they entail multiple parameters to be tuned due to the incorporated amendments. In this regard, an efficient and fast algorithm with a well-founded search ability has been designed in this work. The developed optimizer employs a modified equation from the recent slime mould algorithm (SMA) [34] by incorporating the hyperbolic tangent function as an effective tool to reduce large perturbations during the tracking process. Moreover, the duty cycle updating process allocates half the candidate solutions to inspect the neighborhood of the global optimum solution and the other half to do the same operation within the second-best optimum solution. To guarantee that an optimum region does not get overpromoted, a mechanism is developed in such a way the stored global best and the second best solutions belong to different regions of the PV characteristics. The latter operation is employed only in the first two iterations to ensure a rapid performant exploration process and reduce the chances of local peak stagnation. Once the global peak region has been perceived to the algorithm,

the remaining stages are devoted to focalize the search around it. The new optimizer, which was named the hyperbolic slime mould algorithm (HSMA), is less dependent on random factors, unlike other existing MPPT techniques. In overall, the key contributions and aspects of this work can be outlined as follows:

(i) A novel hyperbolic slime mould algorithm (HSMA) is designed for maximum power point tracking

(ii) The main hallmark of the algorithm lies in its ability to inspect and distinguish the best two peak regions of the search space before eventually converging to the global solution

(iii) The designed optimizer was examined in diverse complex partial shading conditions through simulation trials and validated through an experimental setup consisting of the DSpace controller and a PV emulator

(iv) The conducted performance investigation reveals that the designed HSMA optimizer earned an effective local peak avoidance with high tracking accuracy, tiny perturbations to the operating point, and rapid convergence rate

(v) The designed algorithm proved to be the best-performing algorithm when compared to the well-regarded PSO, GWO, and SMA optimizers in all aspects

The remainder of this paper is set out as follows: in Section 2, a brief overview on PV models and maximum power point tracking is provided. The designed algorithm foundation and its mathematics are explained in Section 3, while Section 4 is devoted to the algorithm working flow and its behavior in maximum power point tracking, with a detailed test case example. Sections 5 and 6 go over the investigated simulation trials and the experimental validation, respectively. In Section 7, a complexity analysis of the designed algorithm is provided with an overall comparison between various MPPT algorithms. A concise conclusion is then given in the last section to outline the key benefits of the designed algorithm.

2. PV Modelling and Maximum Power Point Tracking

The most elementary device that makes up a PV generator is a specially designed semiconductor device called the PV cell. Several models have been developed to simulate the PV cell, among which the single-diode model (SDM) is the simplest and the most common. The equivalent SDM circuit is depicted in Figure 1. It consists of a cell photocurrent source, a shunt resistance R_{sh} to account for leakage current, and a series resistance R_s to account for contacts [35]. Several connections of PV cells constitute a PV module, and several groupings of modules make up a PV array.
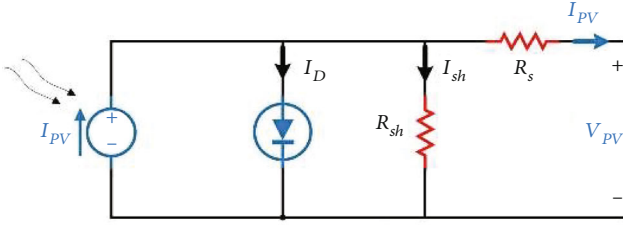
FIGURE 1: The single-diode model for PV cells [35].

The output PV current can be found using

$$I_{PV} = I_{ph} - I_s \left[e^{((q(V_{PV}+R_sI_{PV}))/aKT)} - 1 \right] - \frac{V_{PV} + R_sI_{PV}}{R_{sh}}, \quad (1)$$

where I_o is the diode reverse saturation current, I_{PV} and V_{PV} are, respectively, the current and voltage produced by the PV panel, q is the electron charge ($1.60217662 \times 10^{-19}$ C), a is associated with the PV technology and it is called the diode ideality factor, K is the Boltzmann constant ($1.38064852 \times 10^{-23}$ J/K°), and T denotes the temperature of the p-n junction. To visualize the effects of solar irradiance and temperature, power-voltage curves and current-voltage curves have to be generated using the model equation. Under uniform irradiance, the PV curve is unimodal with a unique maximum, which corresponds to the MPP level. Logically, it is vital that the system operates at this point to maximize its efficiency. In the other hand, when parts of the PV generator do not receive an equal amount of solar irradiance due to shading conditions, the shaded cells are forced to operate in reverse bias mode causing energy losses and hotspot issues. The latter phenomenon which might damage PV devices is often eliminated by integrating bypass diodes with PV strings. At that time, the corresponding PV and IV curves become distorted with multiple peaks as illustrated in Figure 2.

When the PV generator is connected directly to the load, the operating point is fixed by the intersection of load line and the IV characteristic curve. Because usually the intersection does not land on the maximum power point, a power interface has to be inserted between the PV array and the load side of the system. If a buck-boost converter is connected as shown in the arrangement of Figure 3, then the produced output voltage and current are dictated as follows:

$$V_o = \frac{V_{PV}D}{1-D}, \quad (2)$$

$$I_o = \frac{(1-D)}{D}I_{PV}, \quad (3)$$

with D being the duty cycle of the buck-boost converter. The impedance seen by the PV generator which dictates the operating point can then be fixed by the duty ratio as demonstrated in the following equation:

$$R_{Eq} = \frac{V_{PV}}{I_{PV}} = \frac{((1-D)/D)V_o}{(I_oD)/(1-D)} = \left(\frac{1-D}{D}\right)^2 \frac{V_o}{I_o} = \left(\frac{1-D}{D}\right)^2 R_{load}. \quad (4)$$

The latter equation shows how the buck-boost converter can be employed to set the impedance seen by the PV generator and hence the load line intersection. Using a proper algorithm that generates the required duty ratio, the operating point can be varied so that it coincides with the MPP level of the PV array. The employed algorithm is supposed to find the duty cycle value that leads to the maximum power point in the least possible time duration and detects any changes in irradiance levels to start the tracking process again.

3. The Proposed Methodology

3.1. The Slime Mould Algorithm.
The slime mould algorithm was developed based on the special foraging behavior of a single-celled organism known as slime mould. The inspiration was educed from its main nutritional stage during which the organic matters in this organism look around food, ring it and then digest it. The search process of slime mould involves generating a network of veins of distinct densities that extend to multiple food sources. The density is dictated by the goodness and the concentration of the food source. When the vein proceeds towards the food, the biooscillator of slime mould generates a propagating wave through which positive and negative feedbacks are established. An optimal path that connects various food regions would eventually be created. The mathematical model of the slime mould algorithm incorporates this behavior and involves two main mechanisms: approaching food and wrapping food.

3.1.1. Approach Food.
Based on the odor in the air, slime mould approaches the food source with higher concentrations; the following equations are used to model the contraction mode near the food source:

$$\overrightarrow{X(t+1)} = \begin{cases} \overrightarrow{X_b(t)} + \overrightarrow{vb} \cdot \left(\overrightarrow{W} \overrightarrow{X_A(t)} - \overrightarrow{X_B(t)} \right), & r < p, \\ \overrightarrow{vc}\, \overrightarrow{X(t)}, & r \geq p. \end{cases} \quad (5)$$

$\overrightarrow{vb}$ takes on a value within a range of $[-a, a]$ while $\overrightarrow{vc}$ is a parameter that decreases linearly from one to zero. $\overrightarrow{X}$ refers to the location of slime mould at iteration t, $\overrightarrow{X_b}$ denotes the food source with the highest odor concentration ever found, $\overrightarrow{X_A}$ and $\overrightarrow{X_B}$ are two solutions randomly selected from the solution vector, and $\overrightarrow{W}$ represents the weight of slime mould. p is given as follows:
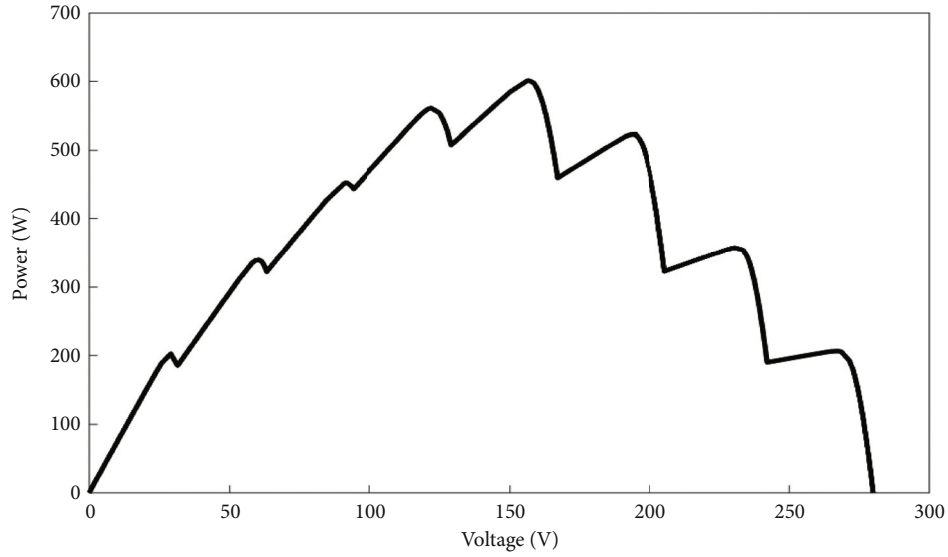
$$p = \tan h|S(i) - DF|, \quad (6)$$

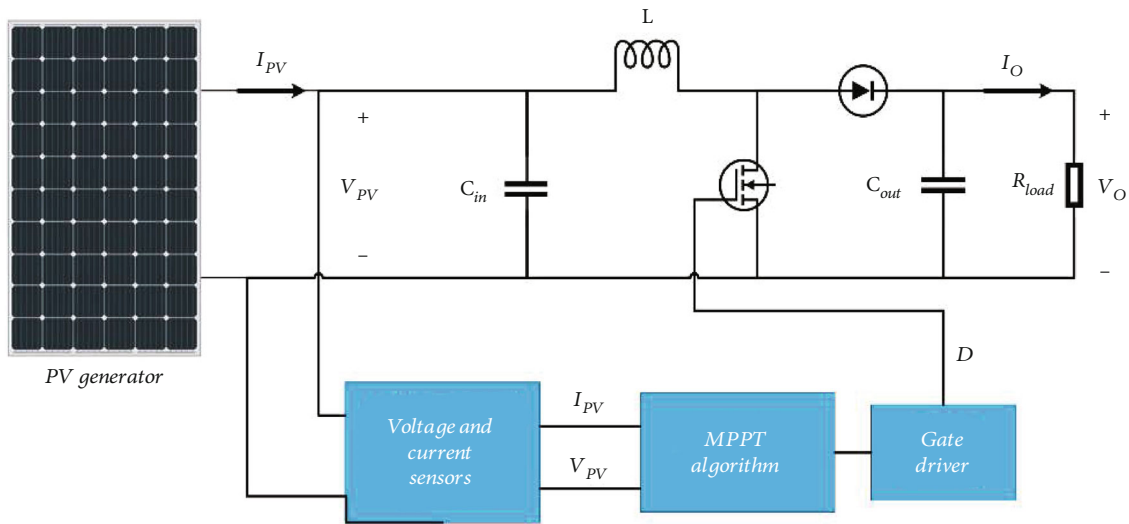FIGURE 2: PV curve of a PV array under partial shading conditions.

FIGURE 3: PV system based on buck-boost converter MPPT.

where $i \in 1, 2, \cdots, n$, $S(i)$ is the fitness value of the ith solution $\overrightarrow{X}$, and DF represents the best fitness obtained so far.

a and $\overrightarrow{W}$ are given as follows:

$$a = \text{arctanh}\left(-\left(\frac{t}{T}\right) + 1\right), \tag{7}$$

$$\overrightarrow{W(\text{SmellIndex}(i))} = \begin{cases} 1 + r.\log\left(\frac{bF - S(i)}{bF - wF} + 1\right), i < \frac{N}{2}, \\ 1 - r.\log\left(\frac{bF - S(i)}{bF - wF} + 1\right), \text{otherwise.} \end{cases} \tag{8}$$

With being the size of the solution vector, r is a random value drawn from the interval [0, 1], bF represents the best fitness value obtained in the current iteration while wF denotes the worst fitness value obtained in the current iteration, and SmellIndex denotes the sequence of fitness values sorted.

$$\text{SmellIndex} = \text{sort}(S). \tag{9}$$

3.1.2. Wrapping Food. Based on the previous mechanism, which simulates the positive and negative feedbacks between the vein thickness and the food concentration, variable weights are employed to quantify the food quantity in a particular region. When the explored region appears to have a low food concentration, the slime mould will decide to leave

```
Initialize the parameters: population size n, Maximum number of iterations T
Initialize the positions of slime mould Xᵢ(i = 1, 2, ⋯, n)
While (ite ≤ T)
        Calculate the fitness of all slime mould;
        Update bestFitness Xb;
        Calculate the weight W using equation (8);
        For each slime mould position:
                Update p, vb, vc;
                Update positions using equation (10);
        End For
        ite = ite + 1;
End While
Return Xb
```

ALGORITHM 1: Pseudocode of the standard slime mould algorithm.

that area to explore other potential food zones. The complete updating mechanism is modeled as follows:

$$\overrightarrow{X(t+1)} = \begin{cases} \text{rand.}(\text{UB} - \text{LB}) + \text{LB}, & \text{rand} < z, \\ \overrightarrow{X_b(t)} + \overrightarrow{vb}.\left(W\overrightarrow{X_A(t)} - \overrightarrow{X_B(t)}\right), & r < p, \\ \overrightarrow{vc}.\overrightarrow{X(t)}, & r \geq p, \end{cases}$$

(10)

LB and UB represent the lower and upper bounds of the search space, and z is constant parameter that is recommended to have the value $z = 0.03$.

The process steps of the SMA can be summarized as follows:

3.2. Hyperbolic Slime Mould Algorithm (HSMA). The slime mould algorithm was successfully employed to tackle a wide range of engineering optimization problems and proved to exhibit good performance. However, in maximum power point tracking, the final output of the optimization process is not the only concern; the applied algorithm needs to be fast, accurate, and exhibit the least possible amount of perturbations. The first and the last aspects arise from the fact that weather conditions might be highly unstable which causes the operating point of the system to fluctuate throughout the day. In turn, the algorithm needs to reinitialize every time the operating point changes, starting the optimization process all over again. For this reason, tracking time is an important factor to make sure that the system settles down at optimum steady conditions as fast as possible. Moreover, the search stage of the algorithm needs to be skillful such that it does not perturb the operating point drastically, causing considerable power losses during the process. Considering the previous facts, the original slime mould algorithm was modified accordingly so that it fits better with MPPT.

Because the first and the third mechanisms of the SMA in equation (10) incorporate high randomness and distant movements, they have been removed in the developed SMA optimizer to reduce perturbations along the search stage. The new version maintains only a refined format of

the second equation from the original SMA optimizer. The refinement employs the hyperbolic tangent function as a tool to minify large displacements that might result from the original equation. The hyperbolic tangent function maps values in the interval [0, 1] nonlinearly to values in the interval [0, 0.76] as shown in Figure 4. The new framework equation is as follows:

$$D_i^{t+1} = Db + S(i) \times a \times \frac{\left|\tanh\left(w(i) \times Db\right) - \tanh\left(G \times D_i^t\right)\right|}{d} \times e^{-\left|Db - D_i^t\right| \times t}.$$

(11)

D_i^t denotes the ith duty cycle at iteration t and $w(i)$ is the corresponding weight value. Db is either the global best solution or the second global best solution. Half the duty cycles will be updated with respect to the global best solution while the second half will be updated with respect to the second global best solution. This is to ensure a performant exploration phase and avoid local peak entrapment. In many circumstances, the first and the second global best solutions might lie within the same region, at that time the algorithm might fall into a local peak area and get stagnated. To avoid such situations and ensure a successful exploration stage, an isolating mechanism is employed in such a way $Dbest_1$ and $Dbest_2$ are of distinct regions.

If $Dbest_1$ is the global best solution, then $Dbest_2$ is the second optimum solution that does not fall within the interval $[Dbest_1 - 0.08, Dbest_1 + 0.08]$. In other words, if any value of the duty cycle produces the second highest power but it falls within the region $[Dbest_1 - 0.08, Dbest_1 + 0.08]$, then it will not be considered as $Dbest_2$. This dynamic region clustering avoids the oversight of one optimum region and reduces early stagnation issues. Once the algorithm has perceived the global peak region, it will be of no use to employ $Dbest_2$ in the remaining search stages. For this reason, Db will take on $Dbest_1$ starting from the 3rd iteration. The above mechanism can be summarized as follows:

$S(i)$ is a flag vector used to decide the direction of the movement. Two solutions are driven to land above Db, and the two remaining solutions are driven to be below Db. This is to ensure an effective search operation within
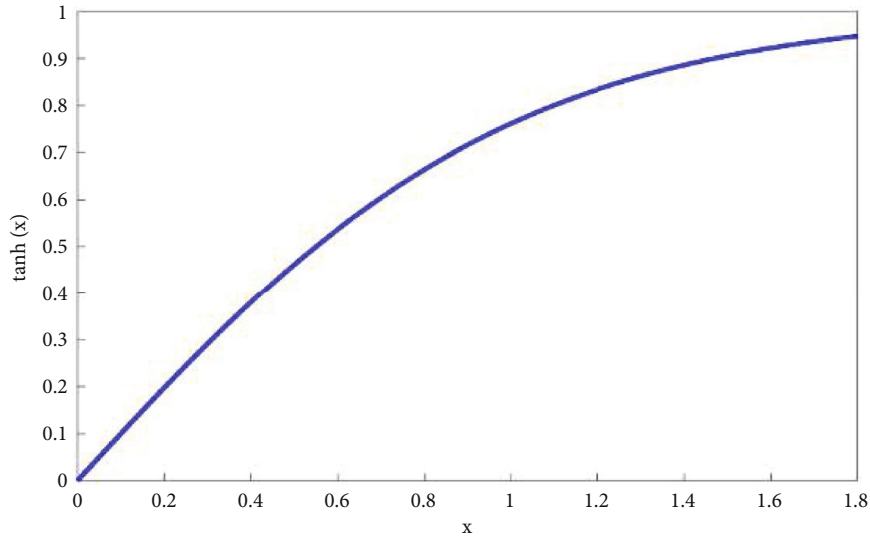
FIGURE 4: The hyperbolic tangent function.

```
if iteration = 1 or iteration = 2
        if i = 1 or i = 2
                Db=Dbest₁
        else
                Db=Dbest₂
        end if
else
                Db=Dbest₁
end if
Where
i is the index of the duty cycle candidate solution (i = 1, 2, 3, 4)
    Dbest₁ : Optimum dutycycle value
    Dbest₂ : Dutycyle value having the highest Power outside the region [Dbest₁ − 0.08, Dbest₁ + 0.08]
```

ALGORITHM 2: Updating mechanism for $Dbest_1$ and $Dbest_2$.

$Dbest_1$ and $Dbest_2$ and avoid overlooking a direction over another. For that matter, the vector S is set as follows: $S = [1, -1, 1, -1]$.

The constant G takes one or two values depending on how close D_i^t to Db according to the following arrangement:

$$G = \begin{cases} 0.8, & \left| Db - D_i^t \right| < 0.01 \text{ and ite} = 2, \\ 0.95, & \left| Db - D_i^t \right| < 0.01 \text{ and ite} = 3, \\ 1, & \text{else.} \end{cases} \tag{12}$$

The employment of this mechanism is to avoid duplication of duty cycle values especially at the exploration phase. The latter phenomenon might cause loss of diversity and early stagnation issues.

d is a damping factor that takes on the value 2 in the second iteration and fixed at 1 in the remaining iterations.

$$d = \begin{cases} 2, & t = 2, \\ 1, & \text{else.} \end{cases} \tag{13}$$

The exponential term in the equation is used to bring down the effect of the large distances between Db and D_i^t. The higher the distance between the two, the lower $e^{-|Db-D_i^t|t}$ it gets along the laps of iterations.

In the third iteration, Db takes on the value of $Dbest_1$ and t in its neighborhood. For the remaining iterations, the search will be narrowed down within the identified foremost region.

During the first iteration, the duty ratios are updated using a slightly different equation:

$$D_i^{t+1} = Db + S(i) \times a \times \text{rand} \times |\tanh(D_{r1}) - \tanh(D_{r2})|, \tag{14}$$

where D_{r1} and D_{r2} are two successive duty ratios randomly chosen from the solution vector. If $D_{r1} = 0.6$, then $D_{r2} = 0.8$. If D_{r1} happens to be $D_{r1} = 0.2$, then $D_{r2} = 0$. This equation assures an effective distribution of the duty ratios around the detected best two solutions. The convergence factor a in (3) of the original version has been modified so that it

decreases exponentially over the lapse of iterations to further boost the convergence rate of the HSMA optimizer:

$$a = e^{-(4t/T)^2}. \qquad (15)$$

The next section provides a profound explanation of the designed algorithm applied to maximum power point tracking.

4. HSMA-Based MPPT

The task in maximum power point tracking is to find the duty cycle value that would result in the highest possible power level the system can deliver. The employed algorithm would be implemented in a microcontroller to serve as the MPP tracker. Based on its mathematical framework, the algorithm in each iteration generates a set of duty cycle values to be transmitted to the DC-DC converter and receives the corresponding voltage and current for fitness evaluation. The duty cycle is then considered as the decision variable that directly affects the power of the system. Accordingly, maximum power point tracking can be regarded as an optimization problem with the following objective function:

$$F(D_i) = P_i, \qquad (16)$$

where D_i is the ith duty cycle generated by the algorithm and P_i is the corresponding PV power. The variable D is constrained within the range $0.1 \le D_i \le 0.9$. If at a certain iteration the distances between the generated duty cycles are very small or the associated power levels are so close, the iterative process will be terminated and the optimum duty cycle will transmitted to the power converter. This convergence criterion is set by the following condition:

$$\frac{|D_i - D_{i-1}|}{D_i} \le 0.01,$$
$$\frac{|P_i - P_{i-1}|}{P_i} \le 0.01. \qquad (17)$$

Moreover, when the optimization stage is stopped, variations in irradiance levels have to be continuously checked by examining the associated power level. If it happens that a change is detected, the optimization process shall be started all over again. The checking condition is as set as follows:

$$\frac{\left| P_{\text{best}}^t - P_{\text{best}}^{t+1} \right|}{P_{\text{best}}^t} \ge 0.02, \qquad (18)$$

where P_{best}^t is the power that corresponds to the optimum duty cycle found during the optimization process. The overall operating flowchart of the HSMA applied on MPPT is illustrated in Figure 5.

4.1. Illustration of the Work of HSMA. In this section, the produced solution trend of the designed algorithm will be visualized iteratively through a case example. A pictorial visualization of the duty ratio trend along the first three iterations is provided in the PV curves of Figure 6 along with the power and duty cycle curves of the HSMA optimizer shown by Figure 7. As shown, the PV characteristics exhibit 4 peaks with the global MPP located at a power level of 703.1 W, while the closest local MPP is around 23 W away and located at 589.5 W in the extreme left. In the initial step, the algorithm sends the initial set of the duty cycles $D = [0.2, 0.4, 0.6, 0.8]$ to the power converter to cover the entire PV curve. In this particular case, the duty cycle value $D_1 = 0.6$ produced the highest power level of 630.5 W (point A), and the algorithm stores it as $D\text{best}_1$. Likewise, $D_2 = 0.2$ produced the second highest power 559.5 W (point B), which makes it $D\text{best}_2$. In the first iteration, equation (14) will be used to convey half the solutions towards the neighborhood of $D\text{best}_1$ and the other half towards $D\text{best}_2$, with one driven above the respective $D\text{b}$ and one below it. The resultant solution vector is $D = [0.652, 0.514, 0.301, 0.129]$ and the associated power of each is recorded. As illustrated in the PV curve of Figure 6(b), the solutions are equally deployed between two distinct regions. After transmitting the updated set, $D_1 = 0.652$ produced 687.8 W (point C), which is the highest value ever found, making it the new $D\text{best}_1$. Without region clustering, the duty ratio $D = 0.6$ becomes the second-best solution as it delivers the second-largest power level. However, by applying the mechanism of region clustering incorporated in the HSMA optimizer, this value of the duty cycle will not be considered as $D\text{best}_2$ since it falls within the same region as $D\text{best}_1$. In other words, $|D\text{best}_1 - 0.6| < 0.08$. In the meanwhile, by neglecting the power associated with $D = 0.6$, $D_3 = 0.301$ produced a power level of 573.1 W (point D) which is the second largest level. Now, since $D_3 = 0.301$ is not within $[D\text{best}_1 - 0.08, D\text{best}_1 + 0.08]$, it is now stored as the updated $D\text{best}_2$. In the next iteration, equation (11) with $d = 2$ will be used to dig around the newly discovered optimum regions. Again, half of the duty cycle set will be conveyed around $D\text{best}_1$, one from above and one from below; the same mechanism is applied for the remaining half, with $D\text{best}_2$. The new solution vector produced by this equation is now $[0.677, 0.633, 0.328, 0.274]$, which are allocated and split between the best-discovered regions as depicted in the PV curve of Figure 6(c). After transmitting the new set of duty cycles, the value $D_1 = 0.677$ reached a new higher level of 703.1 W (point E), making it the new optimal solution $D\text{best}_1$. In the meanwhile, although improvement has been achieved with $D_3 = 0.328$ in the $D\text{best}_2$ region producing a power level of 587.3 W (point F), this is still inferior to the power level delivered by the opposite zone. In turn, the optimum region has now been fully perceived to the algorithm. Starting from the next iteration, which is the third one, $D\text{b}$ is set to $D\text{best}_1$ and all solutions will be conveyed within the recognized optimum region using equation (5) with $d = 1$. Again, half the solutions are landed above $D\text{best}_1$, and the other half is deployed below it. Accordingly, the generated solution vector is $D = [0.682, 0.6671, 0.6961, 0.6627]$ which are assembled in the global MPP level as shown in the last traced PV curve of Figure 6(d).
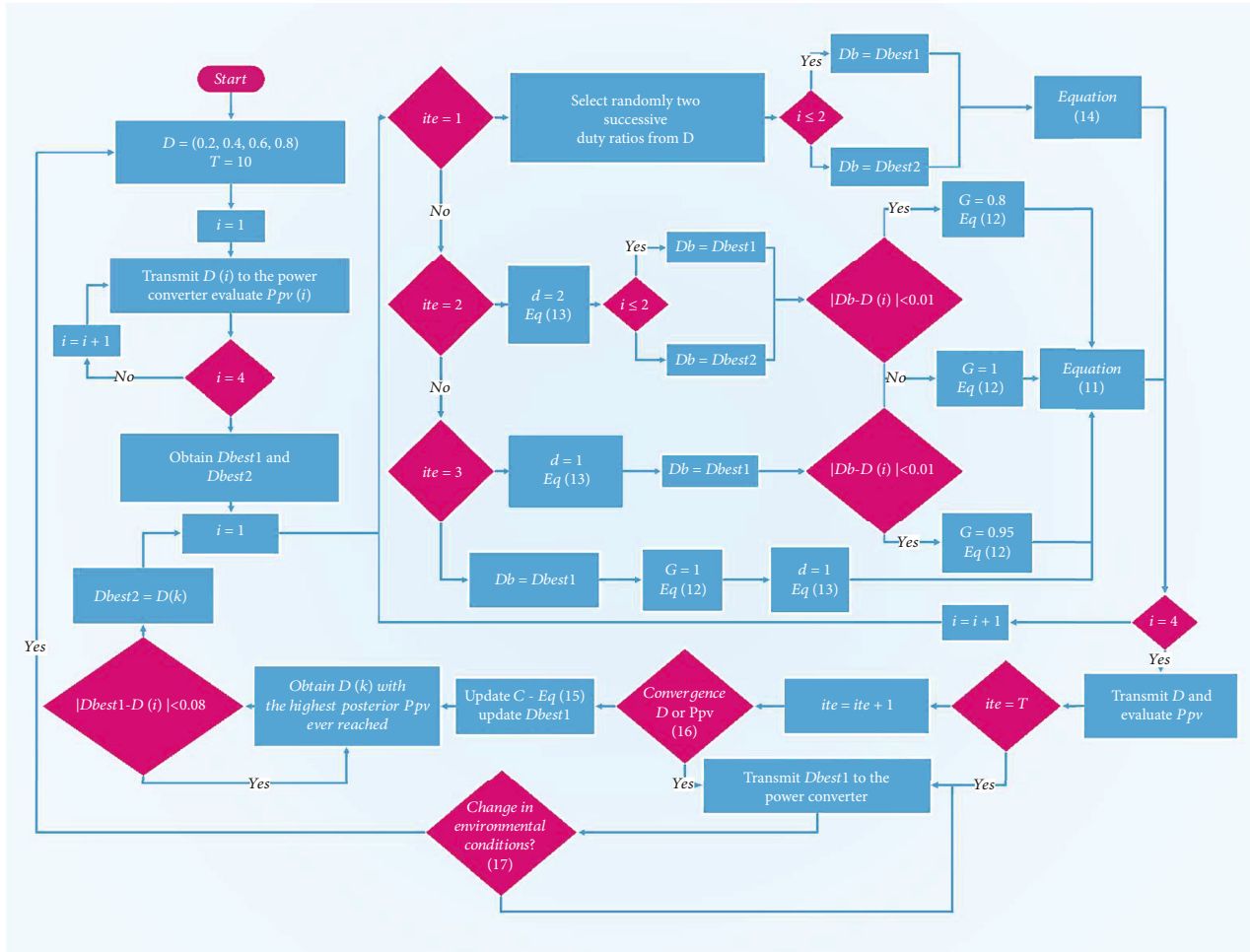
FIGURE 5: Flowchart of the hyperbolic slime mould algorithm-based MPPT.

5. Simulation Results

To examine the performance of the proposed HSMA optimizer, MATLAB/Simulink is employed to simulate a standalone PV system undergoing distinct complex partial shading conditions. The system consists of 8 serially connected PV modules of the same type, a boost converter operated by an MPPT algorithm, and a resistive load. The specifications of the employed PV module are provided in Table 1. The buck-boost converter consists of an input capacitor $C_{in} = 500\,\mu F$, an inductor $L = 150\,\mu H$, and an output capacitor $C_{out} = 0.9\,nF$. The considered cases involve patterns having 5 to 8 peaks with various scenarios of the global peak location, as depicted in the PV characteristics of Figure 8 and Table 2. Three other well-regarded algorithms were applied under the considered cases for the comparative study. The selected parameters for the PSO algorithm are as chosen in [36], while the parameters of the other algorithms were fixed as the default settings in their original articles. All the trials were carried out in MATLAB R2018b and executed on a PC with Intel Core™ I5-1145G7 CPU @ 2.60GHz, 16GB RAM, under Windows 11 64-bit OS. Moreover, for all the considered algorithms, the population size was set to 4 and the maximum number of iterations was fixed at 10. The

sampling time was chosen to be 0.05 s to match it with the experimental work later on.

In the first scenario, the PV generator was subjected to irradiation levels of 950/920/900/500/400/350/320/320 W/m^2. The global MPP is located in the extreme right with a power level of 619.8 W, while the nearest local maximum is at 589.6 W. The resulting power curves and duty ratio adaptation are traced in Figure 9. The HSMA, GWO, and PSO algorithms were all able to recognize the global region and successfully track the GMPP location with an efficiency level of 99.98%. The SMA attained a slightly lower level of 619.6 W, yielding an efficiency level of 99.967%. Despite the similar tracking accuracy, one can easily observe the rapid convergence trend of the HSMA optimizer compared to its contenders. The tracking time was 0.8 seconds which is way smaller than those of the GWO, PSO, and SMA optimizers which consumed 1.7, 1.9, and 2 seconds, respectively. Moreover, it is notable from the power curves and the traced duty cycle that the HSMA generates fewer fluctuations to the operating point leading to lower power losses than those of the other algorithms. This is due to the masterful search strategy which is confined to the two foremost optimum regions, which assists the algorithm in rapidly deciding the global optimal area along the first two iterations.
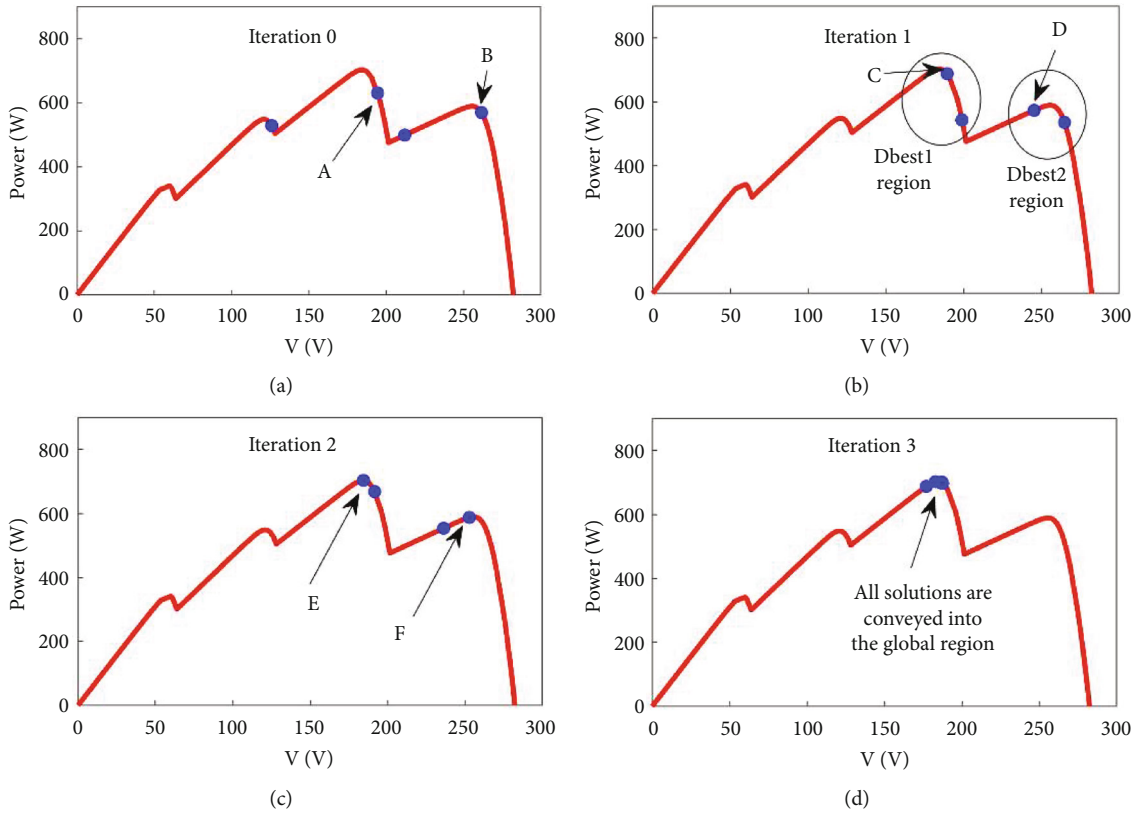
FIGURE 6: Operating point movement of the HSMA optimizer in the case example during (a) iteration 0, (b) iteration 1, (c) iteration 2, and (d) iteration 3.
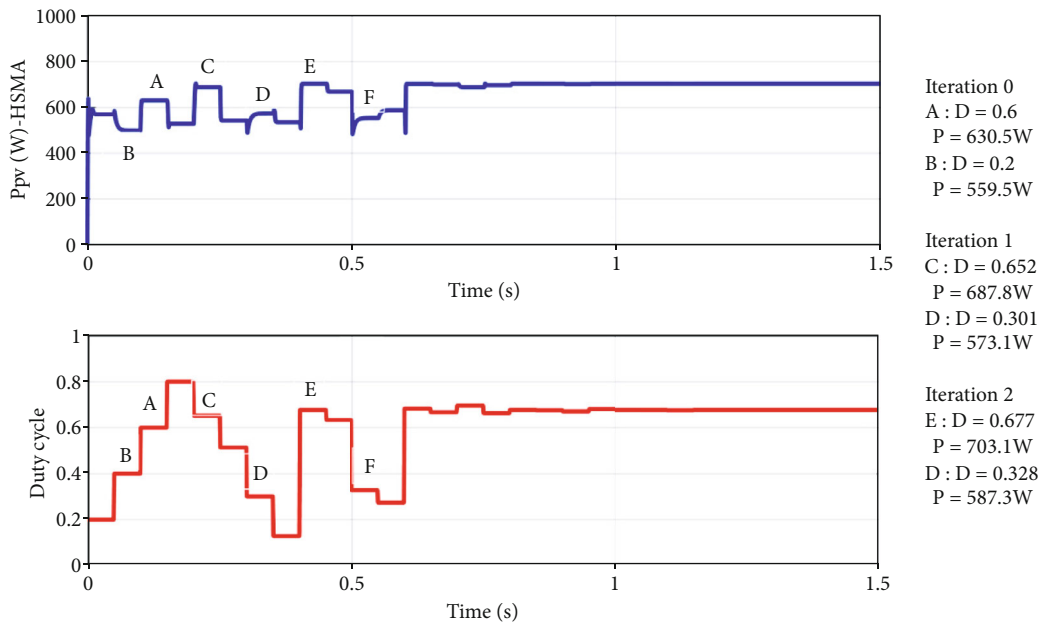

FIGURE 7: Power and duty cycle curves of the HSMA optimizer in the case example.

In the second scenario, the PV generator receives irradiance levels of 50/400/400/500/800/800/1000/1000 W/m^2 resulting in a 5-peak PV curve. The corresponding global MPP is located at a power level of 722.65 W while the near-

est local peak provides 681.2 W. The resulting power curves and duty ratio adaptation are provided in Figure 10. It is revealed from the graphs that except for the HSMA optimizer, the GWO, PSO, and the original SMA got entrapped

TABLE 1: Specifications of the employed PV module.

Module	1Soltech 1STH-215-P	Open circuit voltage (V_{OC})	36.3 V
Maximum power P_{MP}	213.5 W	Short circuit current (I_{SC})	7.84
Voltage at P_{MP} (V_{MPP})	29 V	Cells per module	60
Current at P_{MP} (I_{MPP})	7.35 A		
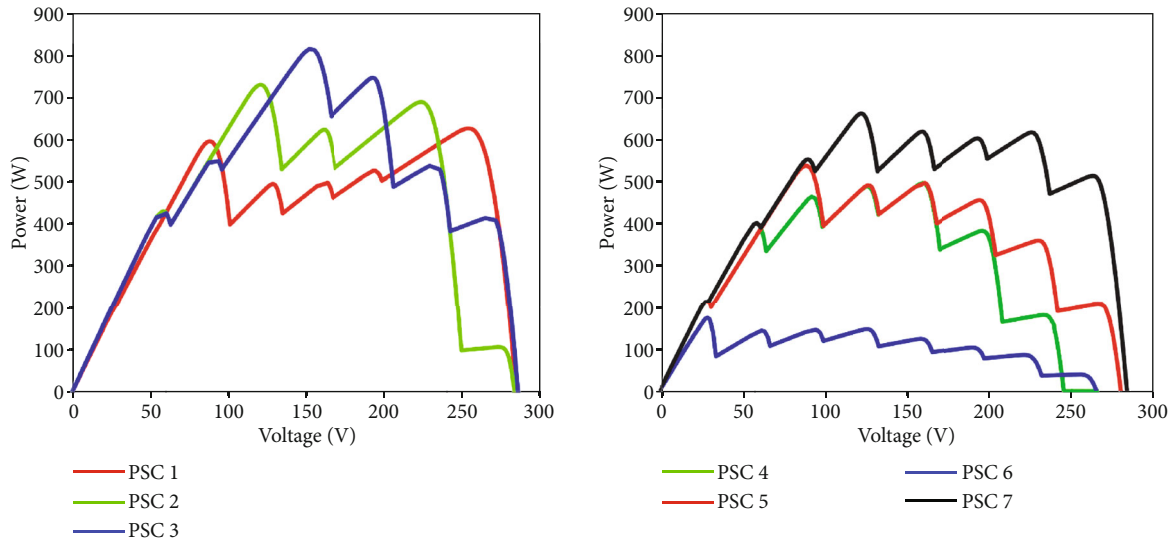
FIGURE 8: PV curves of the investigated partial shading conditions.

TABLE 2: Details of the investigated partial shading conditions.

PSC case	Pattern (W/m²)	Number of peaks	GMPP (W)	GMPP location	LMPP 1 (W)
PSC1	950/920/900/500/400/350/320/320	5	619.8	Right	589.6
PSC2	50/400/400/500/800/800/1000/1000	5	722.65	Middle	681.6
PSC3	1000/1000/800/700/700/500/300/200	6	806.8	Middle	738.9
PSC4	1000/900/600/0/500/400/250/200	7	492	Middle	484.7
PSC5	1000/300/800/800/500/400/200/100	7	532.2	Middle	492.4
PSC6	800/300/200/150/100/70/50/20	8	171.7	Left	145.1
PSC7	1000/900/800/600/500/400/350/300	8	655.7	Middle	486

at the local region. In this scenario, it happened that when transmitting the initial duty cycles, the one with the value $D = 0.2$ produced a higher power than the ones with $D = 0.6$ and $D = 0.8$, which are supposed to belong to the global optimum zone. For that reason, the SMA, GWO, and PSO algorithms got rapidly sucked into the 681 W region. Although the standard SMA optimizer attempted to escape from the local region at the seventh iteration, the attempt was insufficient. The HSMA on the other hand could easily differentiate between the regions and eventually converge towards the global zone. This early recognition is due to the mechanism of exploring the neighborhood of the best two regions, giving both regions chances to reveal where the global optimum zone is located. In terms of convergence time, the HSMA is faster at 0.8 s followed by the original

SMA at 1.1 seconds and the PSO and GWO algorithms at 1.4 and 1.6 seconds, respectively.

In the third scenario, the system undergone a PSC pattern having irradiance levels of 1000/1000/800/700/700/500/300/200, resulting in a characteristic curve of 6 peaks. The associated global peak is located at 806.8 W in the middle, while the first local peak is around 70 W far from it. The resulting power curves and duty ratio adaptation are provided in Figure 11. Although the HSMA, PSO, and SMA scored the highest efficiency level of 806.5 W, the developed optimizer's tracking time, which was 0.8 s, was way shorter than those of its contenders. In effect, both the PSO and the SMA optimizers consumed around 1.8 s, while the GWO algorithm was the worst with a 2 s tracking time. It can be observed from the power curves that the HSMA
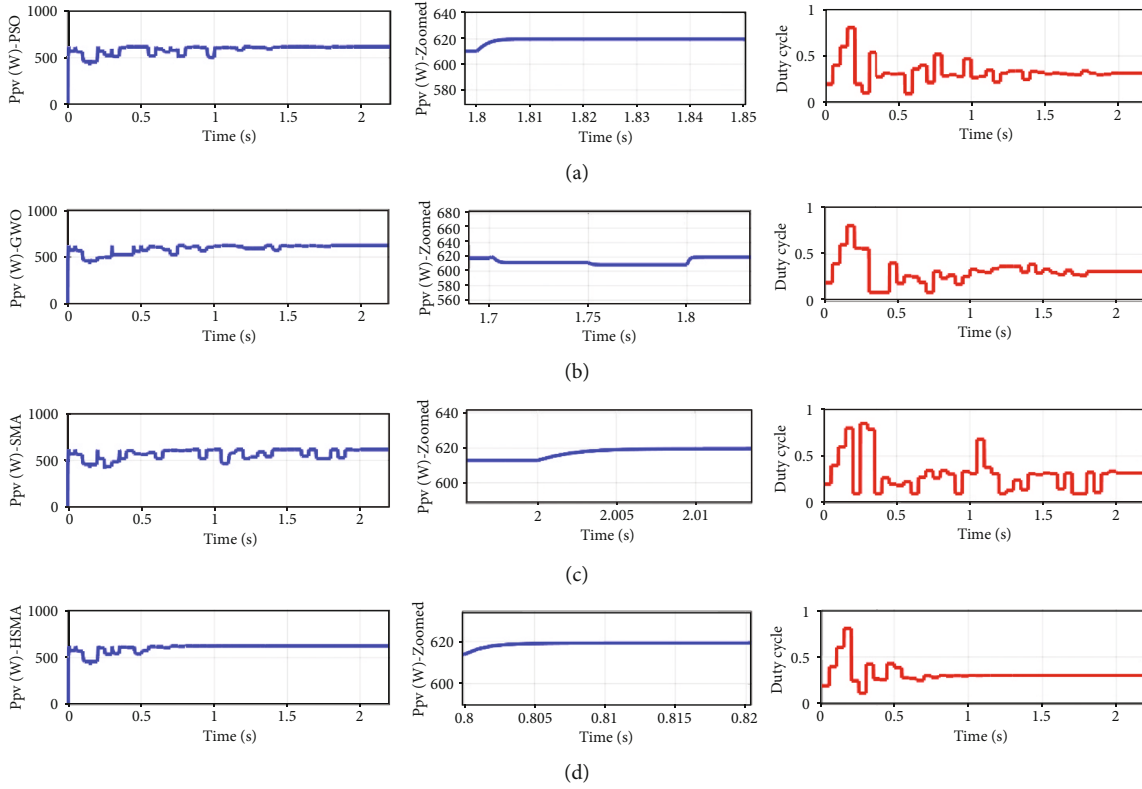
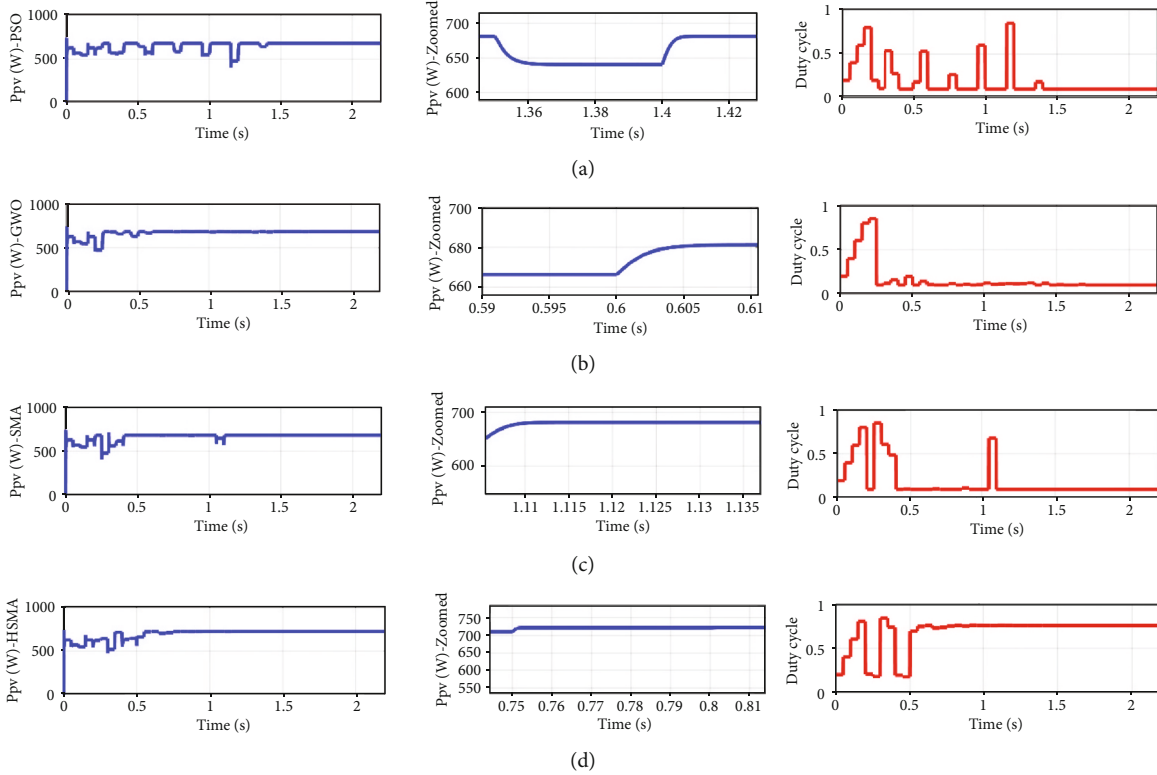Figure 9: Power and duty cycle curves during PSC1 for (a) PSO, (b) GWO, (c) SMA, and (d) HSMA.

Figure 10: Power and duty cycle curves during PSC2 for (a) PSO, (b) GWO, (c) SMA, and (d) HSMA.
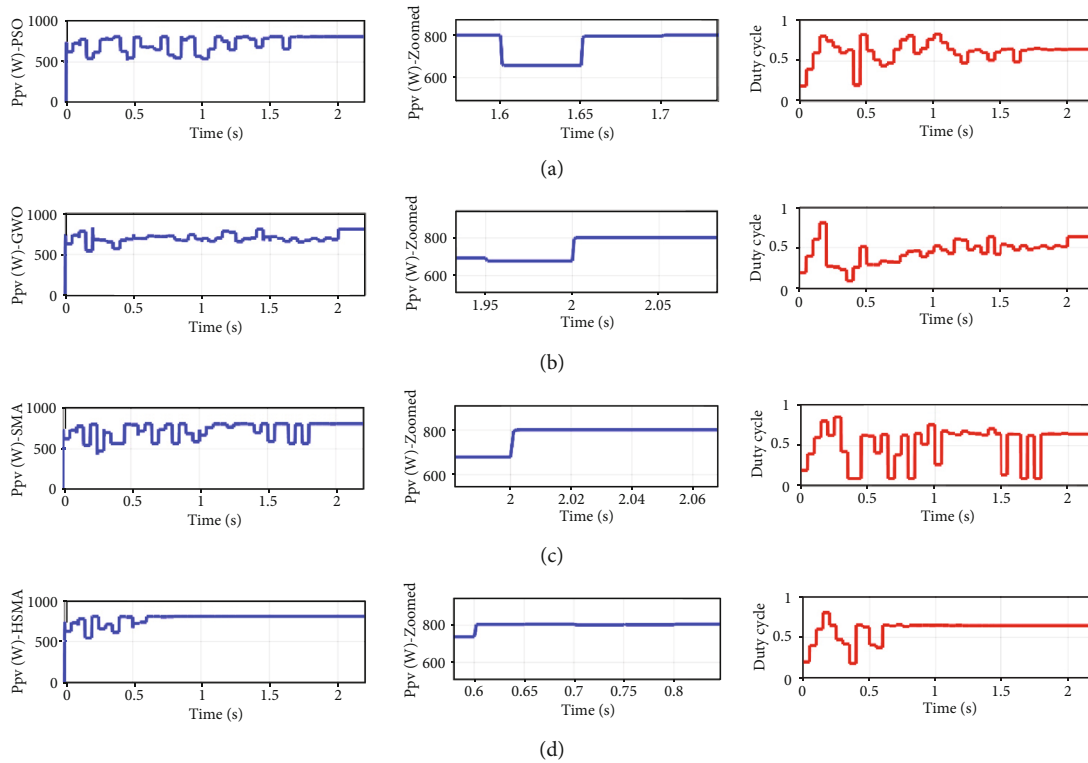
FIGURE 11: Power and duty cycle curves during PSC3 for (a) PSO, (b) GWO, (c) SMA, and (d) HSMA.

optimizer exhibits the least amount of fluctuations compared to those of the GWO, PSO, and SMA. This is due to the rapid decision-making attribute of the guided exploration stage and by which the search process was not strayed away from the optimal peak regions.

The fourth trial involves a profile having levels of 1000/900/600/0/500/400/250/200 W/m², and the corresponding PV curve consists of 7 peaks. The global peak is at 492 W, and the associated duty cycle value is 0.356, while the closest local peak is only 7 W away from it, making the case so challenging to handle. The associated delivered power curves and the generated duty ratio values are shown in Figure 12. In the initial step, the value $D = 0.4$ produces 470 W while $D = 0.6$ produces a higher level of 481.2 W, causing an entrapment to the MPPT algorithm. Despite the troublesome pattern, the designed HSMA optimizer effectively conveyed the operating point to the global maximum level resulting in a 99.99% efficiency. The dynamic region clustering enabled the algorithm to avoid entrapment into the closest local zone with rapid and masterful decision-making. As can be observed, the GWO algorithm could manage to achieve identical efficiency with the HSMA optimizer; however, this was at the expense of high fluctuations and sluggish convergence. In effect, the HSMA was again the fastest algorithm, with 0.8 seconds, followed by the GWO algorithm, which took 1.8 seconds to converge. In the meanwhile, the PSO and the SMA optimizers failed to recognize the global region and got entrapped into a local MPP zone.

In the fifth case, the PV array is exposed to irradiance levels of 1000/300/800/800/500/400/200/100 W/m². The resulting 7-peak PV curve exhibits a global maximum located near the extreme left with a power level of 532.2 W, while the first local peak was made close at a level of 493 W. The corresponding power curves and duty ratio adaptation are provided in Figure 13. Similar to PSC2 and PSC3, the global region cannot be revealed after transmitting the initial set of duty cycles. In turn, the GWO and PSO algorithms failed to recognize the optimum zone and rapidly got stuck at the 493 W level. The SMA has also got stuck in that zone in the first 4 iterations; yet, due to the reinitialization mechanism of that algorithm, it could manage to escape into the global region afterwards. However, the exploitation phase could only achieve a power level of 523 W, which is still far off the GMPP location resulting in poor efficiency and slow convergence. In the meantime, due to the masterful exploration mechanism of the HSMA optimizer, the global region was spotted in the first iteration and took 0.8 seconds to converge.

In the sixth experiment, the PV curve consists of 8 peaks, with the global max located at the extreme left at a power level of 171.7 W. The resulting power curves and duty ratio adaptation are provided in Figure 14. All algorithms could manage to successfully land at the global peak level with identical efficiency of 99.99%. However, as with the other cases, the HSMA optimizer provides the best convergence trend with 0.8 seconds tracking time and the slightest amount of fluctuations.

The last trial involves an 8-peak PV curve by exposing the system to irradiance levels of 1000/900/800/600/500/400/350/300 W/m². The global peak is located at the extreme right with a power level of 655.7 W, while the nearest local maximum is located at a power level of 486 W. The resulting
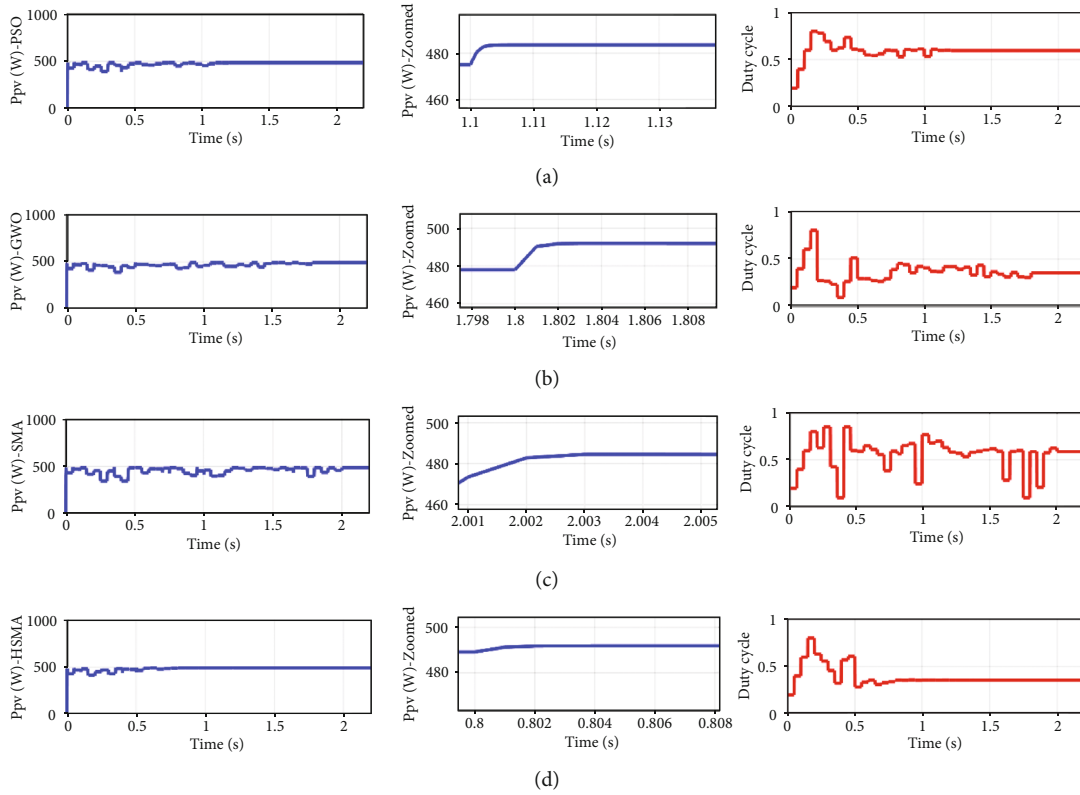
Figure 12: Power and duty cycle curves during PSC4 for (a) PSO, (b) GWO, (c) SMA, and (d) HSMA.
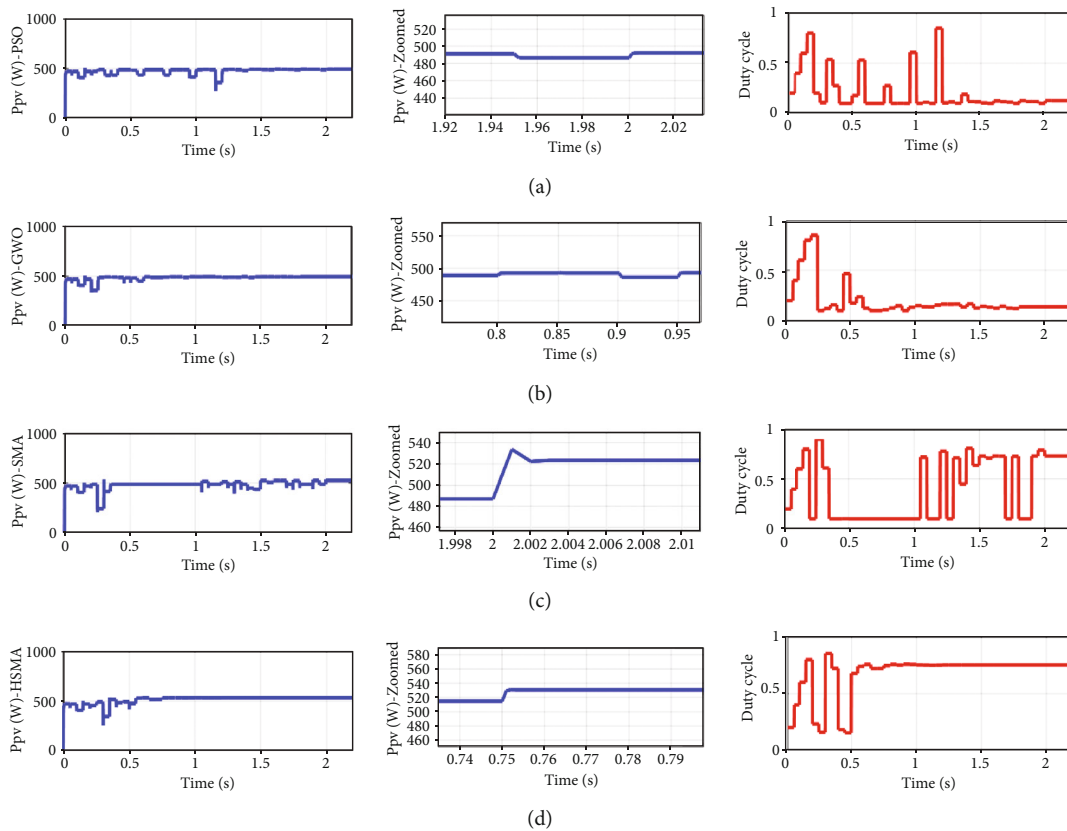

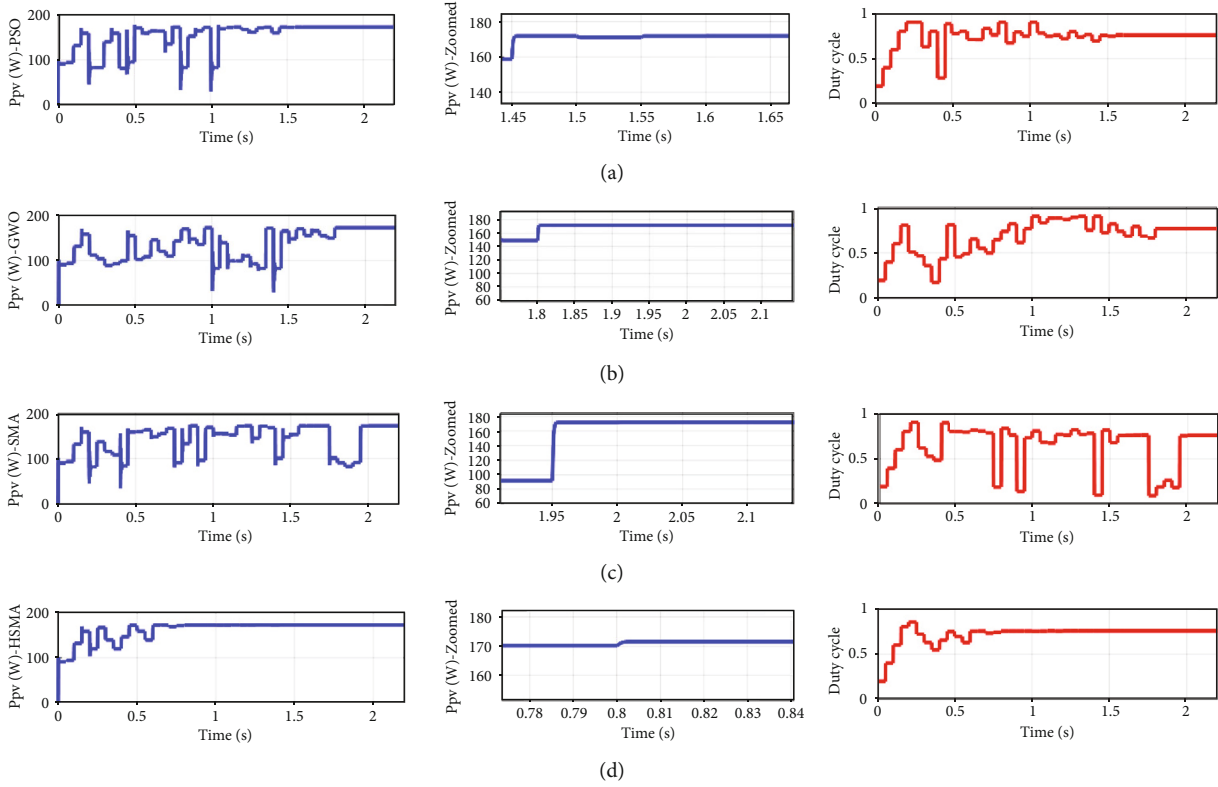Figure 13: Power and duty cycle curves during PSC5 for (a) PSO, (b) GWO, (c) SMA, and (d) HSMA.

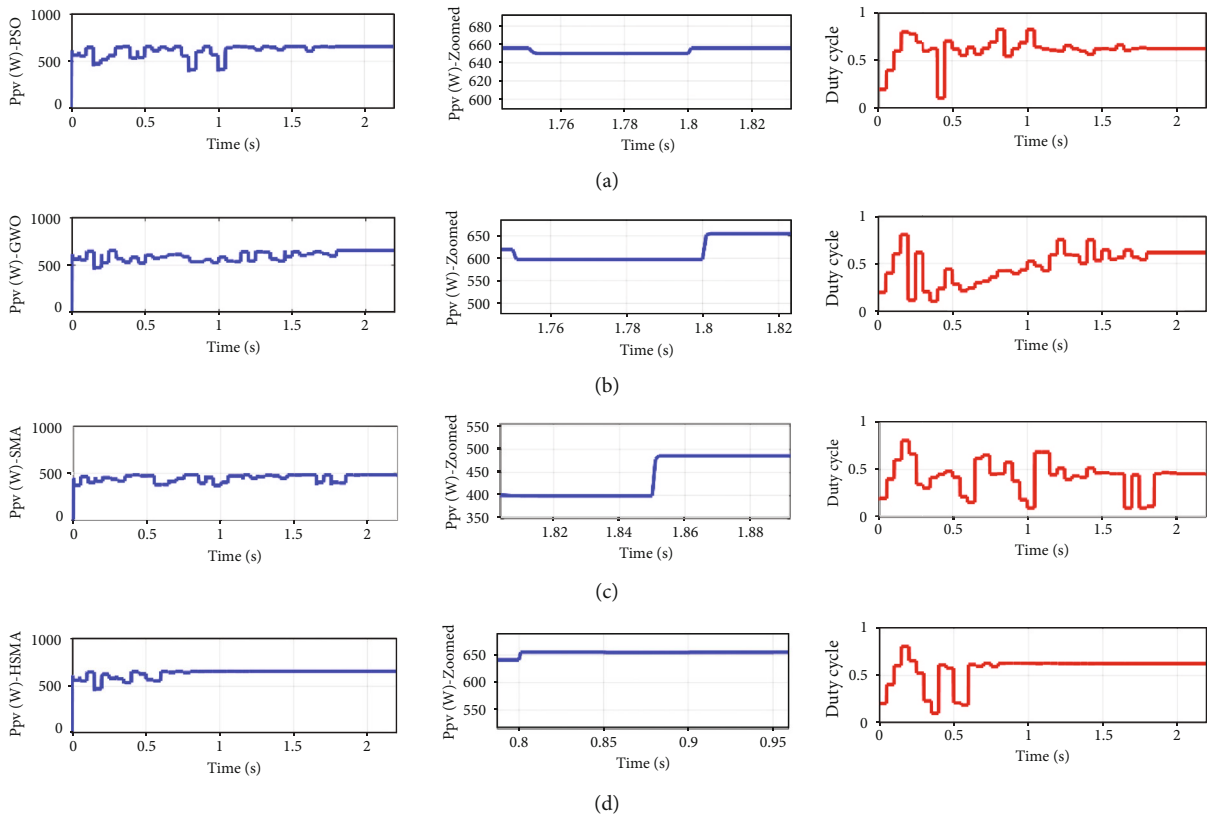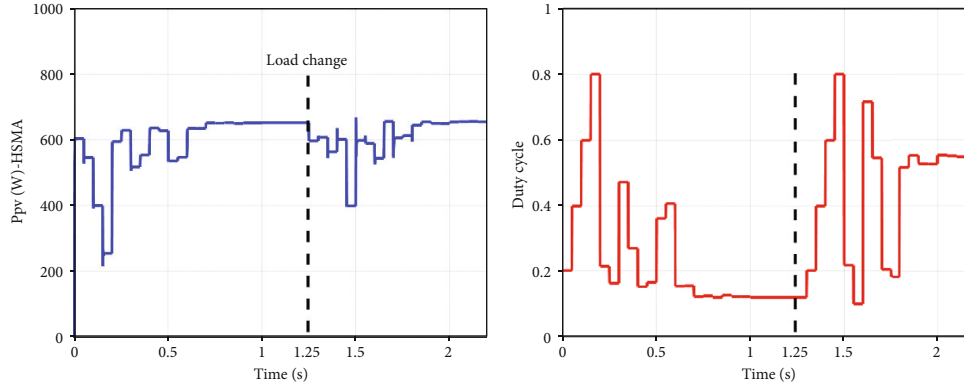FIGURE 14: Power and duty cycle curves during PSC6 for (a) PSO, (b) GWO, (c) SMA, and (d) HSMA.

FIGURE 15: Power and duty cycle curves during PSC7 for (a) PSO, (b) GWO, (c) SMA, and (d) HSMA.

FIGURE 16: Power and duty cycle curves during PSC7 of the HSMA optimizer under dynamic load conditions.

power curves and the traced duty ratio progression are provided in Figure 15. It happened that the HSMA, GWO, and PSO algorithms were able to recognize the global optimum region while the standard SMA optimizer failed in this task. The HSMA and PSO algorithms attained identical power levels of 655.6 W and a corresponding efficiency of 99.98%; however, the GWO achieved 654.6 W resulting in a lower efficiency of 99.83%. Despite their similar accuracy scores, the tracking process of the developed HSMA optimizer is way better than those of its competitors. This is perceivable from its respective power curves from which one can observe smaller convergence time, faster decision-making, and fewer perturbations to the operating point. Moreover, the GWO and PSO algorithms' search process generates previously produced and evaluated solutions causing sluggish convergence and poor accuracy.

To assess the HSMA optimizer in achieving identical efficiency levels at the same irradiance, it was tested under varying load conditions. The system was exposed to the last PS conditions with a load change from $50\,\Omega$ to $25\,\Omega$ after 1.25 seconds. It can be seen from the resulting curves in Figure 16 that the algorithm was able to recognize the change in the power level and reinitialized the search starting from the next sampling cycle. Once again, the algorithm maintained its behavior during the search process with 99.98% efficiency in both load conditions and 0.8 seconds tracking time.

6. Experimental Validation

To support the results obtained through the simulation trials, the HSMA optimizer was examined on an experimental setup shown in Figure 17 for real-time performance investigation. The system is made up of a PV array emulator employed to generate the intended partial shading conditions, a buck-boost converter, and DSpace (D1104) as the controller that transmits the generated PWM signals to the gate driver. The Chroma 62150H PV emulator was used to setup a PV generator consisting of 6 modules connected in series. The selected solar module is the SunPower SPR-305-WHT having the following characteristics: $V_{mpp} = 10.9\,V$, $I_{mpp} = 5.59\,A$, $V_{oc} = 13.1\,V$, and $I_{sc} = 5.92\,A$. The
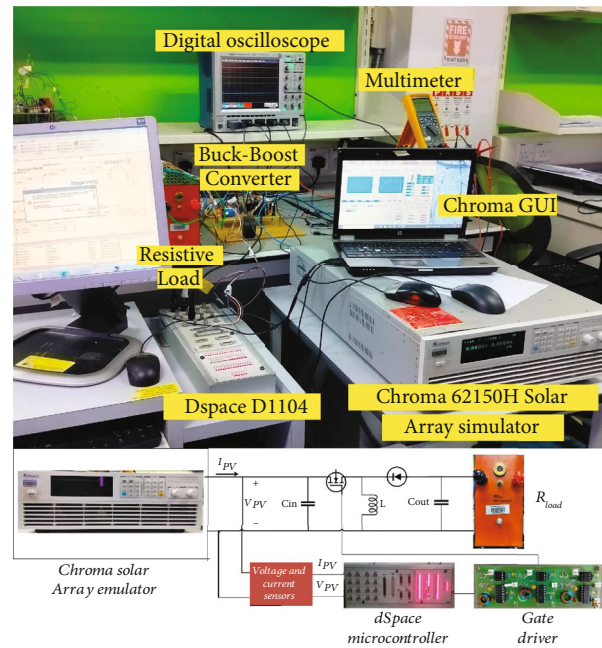

FIGURE 17: Employed experimental setup.

generated voltage V_{PV} and current I_{PV} from the PV simulator were measured by a voltage (LEM LV-25-P) sensor and a current (LEM LA-25-NP) sensor which provide readings to the ADC pins of the DSpace microcontroller. The employed boost converter consists of an input capacitor $C1 = 1200\,\mu F$, an output capacitor $C2 = 550\,\mu F$, an inductor $L = 470\,\mu H$, and a variable load resistor fixed at $R = 20\,\Omega$ with the switching frequency set to 20 kHz. Based on the buck-boost converter settling trend, the sampling time was selected to be 50 ms to provide accurate readings of voltage and current to the microcontroller. This section is devoted to the analysis of the algorithm records on the used experimental setup.

In the first scenario, the system receives solar irradiance levels of 1000, 1000, 900, 800, 700, and $600\,W/m^2$ resulting in a PV curve of 5 peaks. The global peak is located at the extreme right with a power level of 261.51 W as indicated in the screen of the PV emulator. The resulting power curves
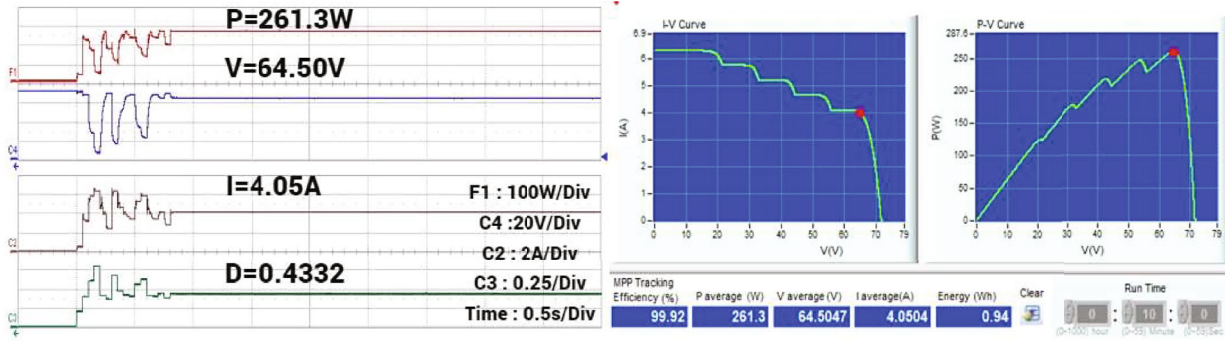
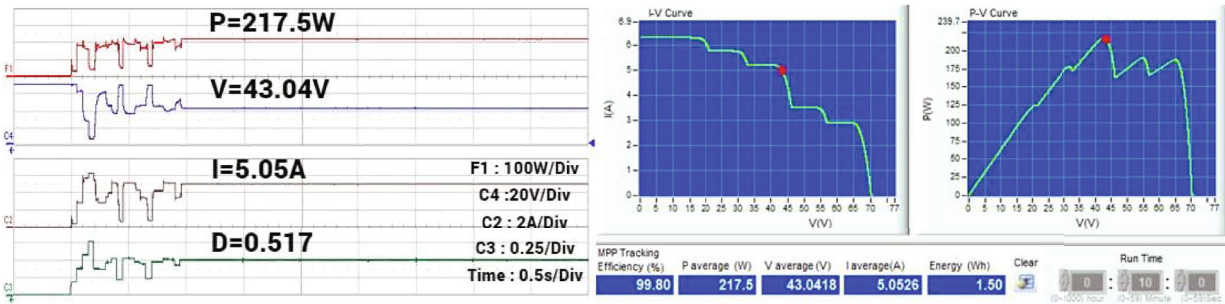Figure 18: HSMA resulting curves along experimental trial PSC1.

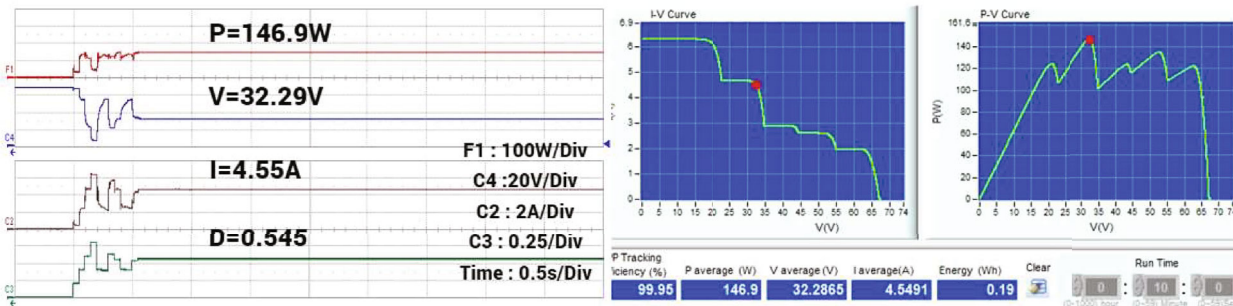Figure 19: HSMA resulting curves along experimental trial PSC2.

Figure 20: HSMA resulting curves along experimental trial PSC3.

and duty cycle progression are provided in Figure 18. The red point on the PV and IV curves corresponds to the steady state reached after the optimization process. The algorithm was able to stand at a power level of 261.3 W with 99.92% efficiency within 0.8 seconds, matching the simulation records. Disregarding the first fluctuations which correspond to the initial set of duty cycles, it is apparent that the algorithm induced tiny perturbations during the optimization process before steady state. This feature is attributed to the smooth exploration phase that allows digging around the best two solutions before deciding which of which the optimum region is.

In the second test case, the system is exposed to irradiance levels of 1000, 1000, 900, 800, 500, and 400 W/m^2. The associated 5-peak PV curve is shown in Figure 19, with an MPP level of 217.5 W. As recorded in the figure, the algorithm successfully located the GMPP region with 99.8% efficiency. Although the tracking time was 0.95 s which is a bit longer than that of the other cases, the duty cycle perturbations in the last iterations are very tiny with unnoticeable power fluctuations during these moments.

The PV and IV curves corresponding to the third trial are provided in Figure 20. The global MPP is located in the middle with power level of 146.9.9 W. Again, the HSMA optimizer was able to convey the operating point into the GMPP with 99.95% efficiency within 0.6 seconds. It is perceivable from the duty cycle progression that the algorithm was able to quickly decide which region is the optimum one, resulting in a few and tiny perturbations and hence small power losses.

In the fourth case, the global MPP is located in the extreme left of the PV curve as depicted in Figure 21. The system is exposed to irradiance levels of 1000, 1000, 350, 300, 150, and 100 W/m^2. The algorithm was able to attain a power
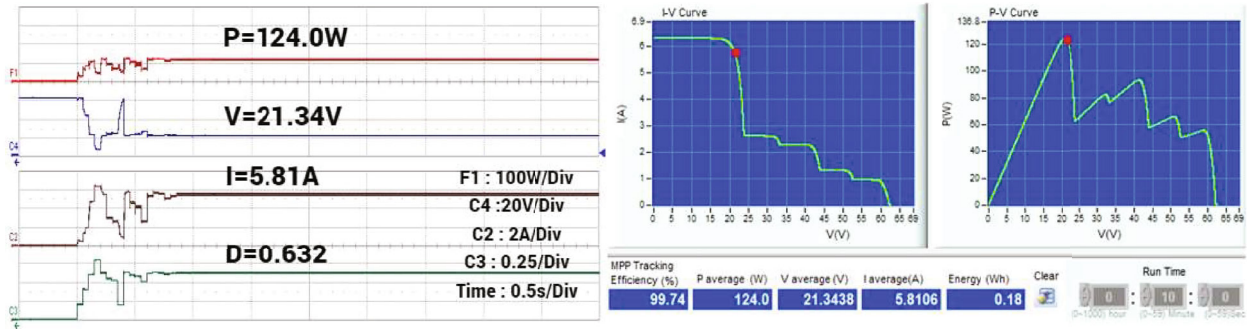
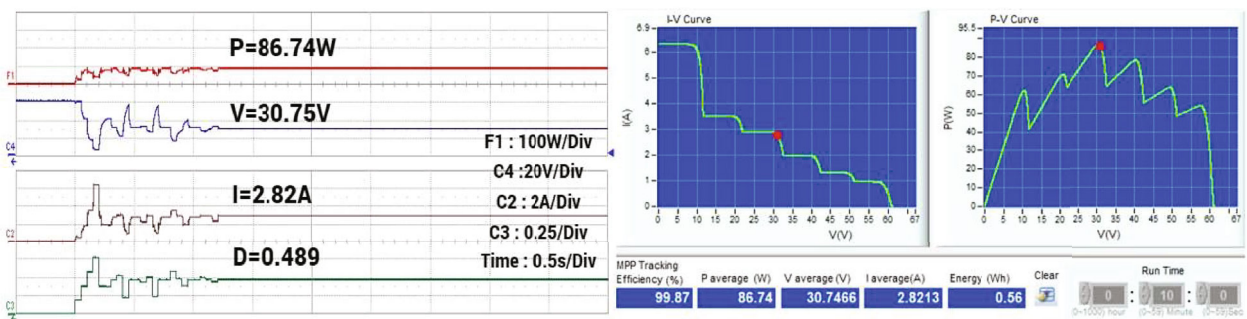FIGURE 21: HSMA resulting curves along experimental trial PSC4.

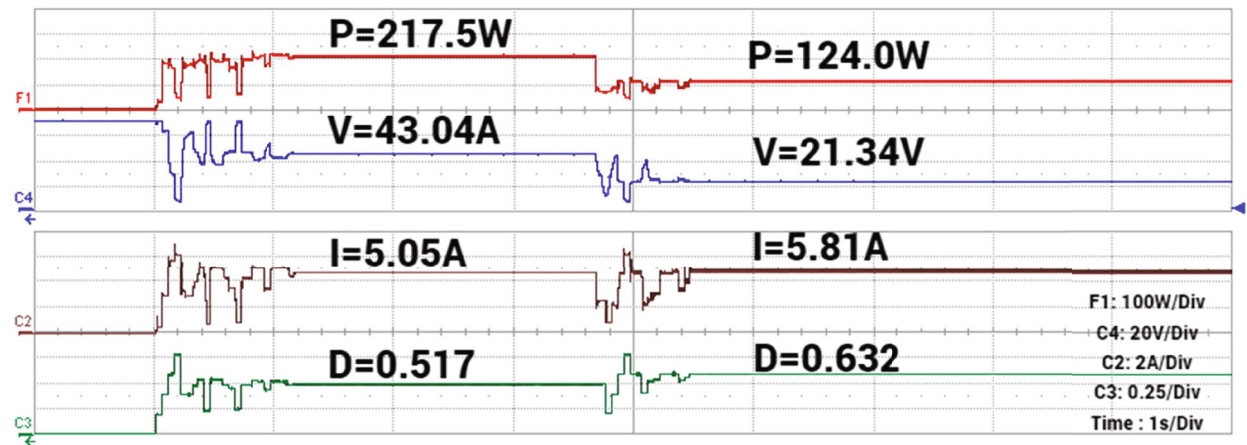FIGURE 22: HSMA resulting curves along experimental trial PSC5.

FIGURE 23: HSMA resulting curves along experimental trial PSC2-PSC4.

level of 124 W out of 124.3 W resulting in 99.75% efficiency. The tracking time was 0.8 seconds, which is again in accordance with the one of the simulation part.

The fifth experiment involves 6 peaks resulting from exposing the PV generator to irradiance levels of 1000/500/ 400/250/150 and 100 W/m². The global peak is located in the middle at a power level of 86.86 W as shown in Figure 22. The HSMA optimizer was able to deliver 86.74 W resulting in 99.87 W. The algorithm this time took a bit longer to settle down and consumed 1.2 seconds to con-

verge. Despite this slower convergence, the perturbations during the tracking stage are small and the corresponding power fluctuations are small.

In the last experimental trial, the system was exposed to a dynamic irradiance of two partial shading patterns. The first pattern is the same as PSC2 and the second pattern is set as PSC4. This experiment is important to testify the algorithm performance in detecting irradiance changes which usually occur in practice. As can be perceived from the outcomes of Figure 23, the HSMA optimizer was able to
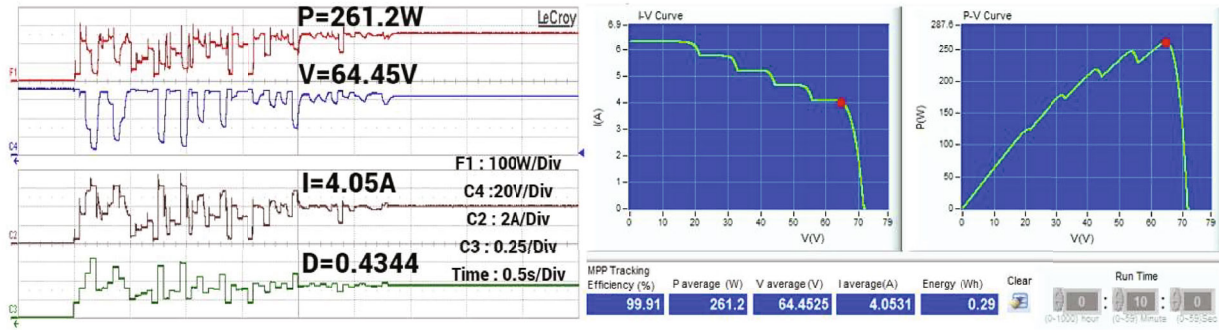
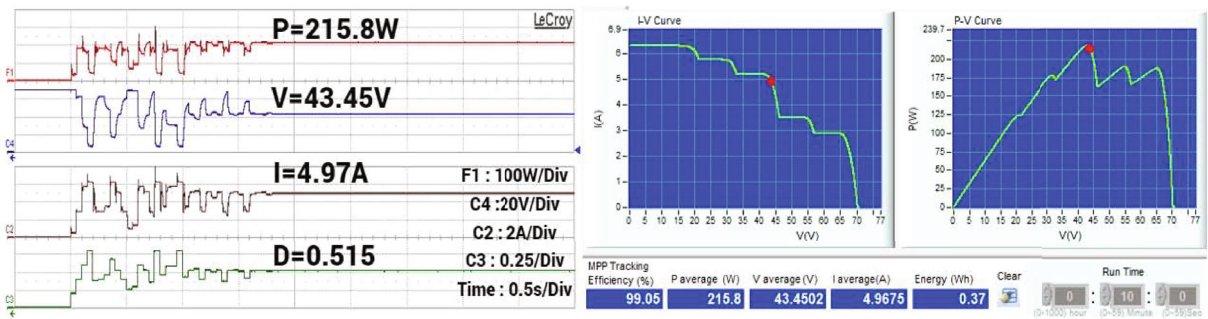FIGURE 24: PSO resulting curves along experimental trial PSC1.

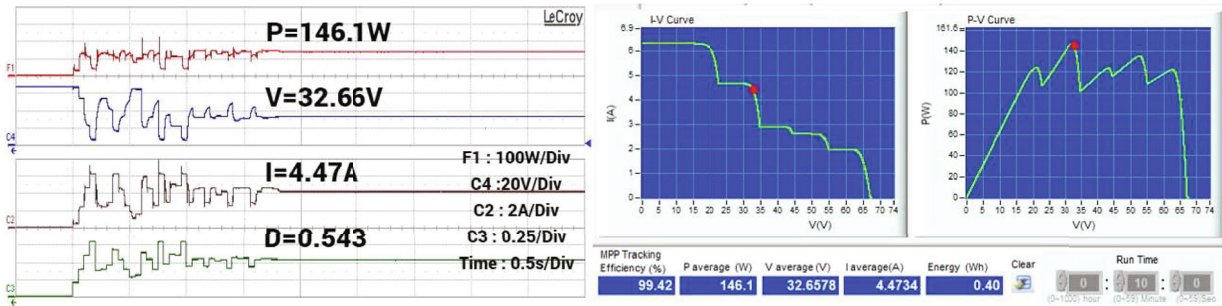FIGURE 25: PSO resulting curves along experimental trial PSC2.

FIGURE 26: PSO resulting curves along experimental trial PSC3.

reinitialize the tracking process immediately once the change occurred. Along the first pattern, the algorithm took around 1.1 seconds to converge, while in the second case, it consumed only 0.6 seconds to settle down at the global optimum operating point.

To support the rival and superior performance of the HSMA optimizer, the previously considered algorithms were implemented on the same experimental setup and conditions. The produced power, current, voltage, and duty cycle graphs of each algorithm are provided in Figures 24–38. The detailed outcomes of all algorithms along the investigated experimental cases are reported in Table 3. In overall, the results are much the same as the ones obtained during the simulation trials. Clearly, a high number of fluctuations

and jumps characterize the power curves produced by the PSO, GWO, and the SMA optimizers before arriving at steady-state conditions. This highly random and unguided search process caused lots of power perturbations and eventually sluggish tracking speed. The HSMA optimizer in the other hand could achieve a very small tracking time of 0.6 seconds, while the largest recorded time was 1.2 seconds. With the investigated cases, the HSMA optimizer settles down on average within 0.87 seconds, which is nearly 4.3 iterations. In terms of tracking accuracy, the designed algorithm was able to achieve experimentally an efficiency level as high as 99.95% and 99.87% on average, which is very promising, bearing in mind its rapid convergence trend and its low fluctuations. In general, the reported results of
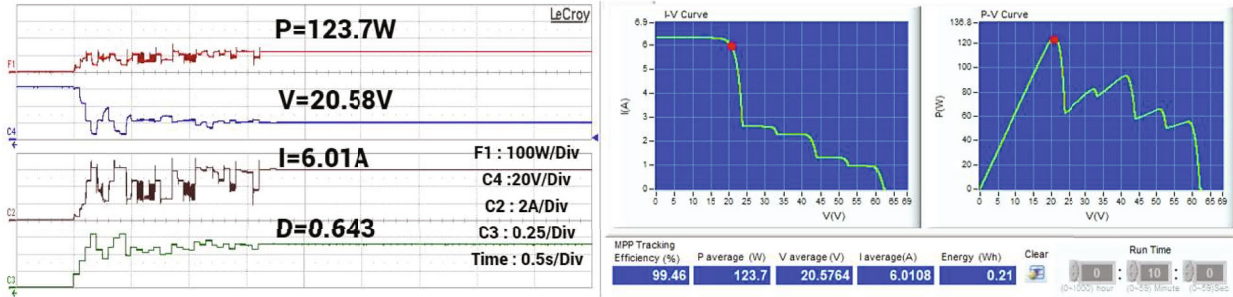
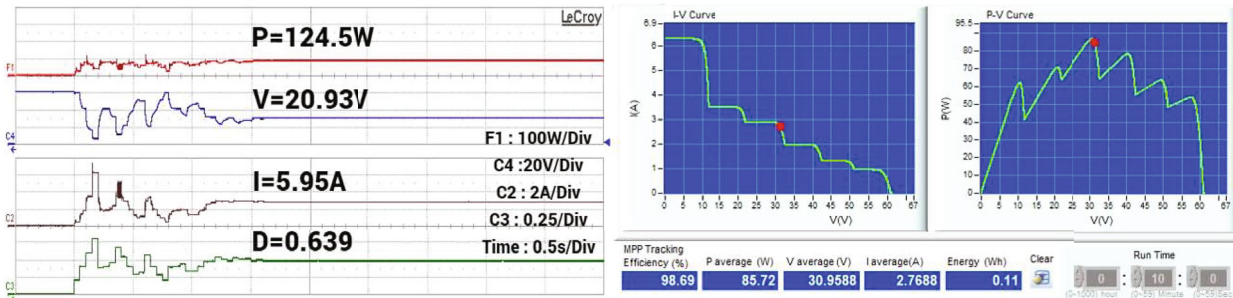Figure 27: PSO resulting curves along experimental trial PSC4.

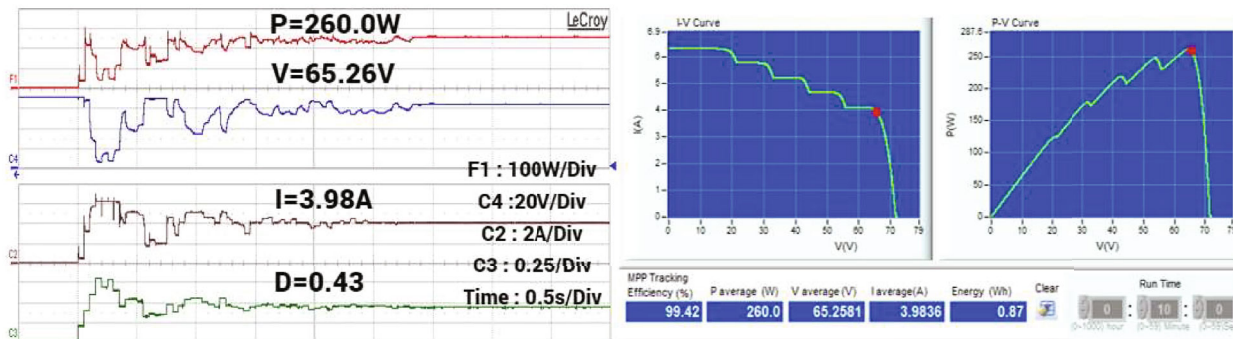Figure 28: PSO resulting curves along experimental trial PSC5.

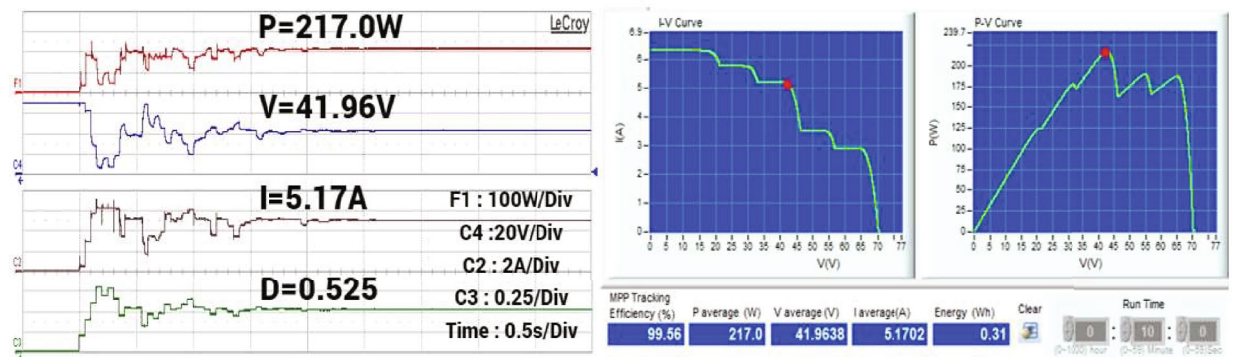Figure 29: GWO resulting curves along experimental trial PSC1.

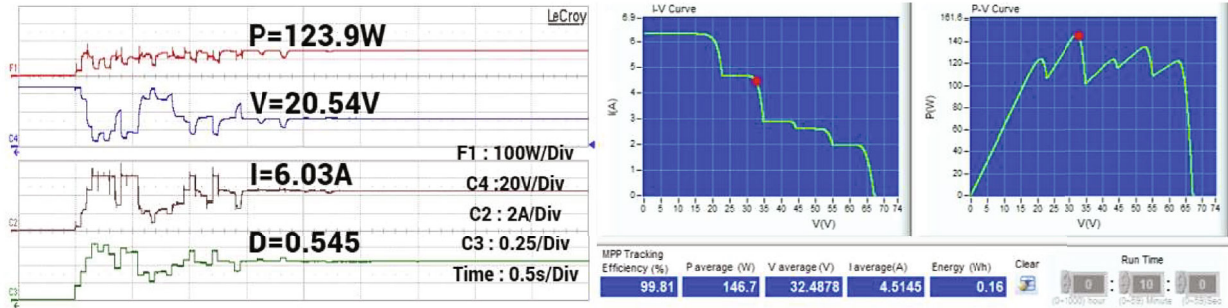Figure 30: GWO resulting curves along experimental trial PSC2.

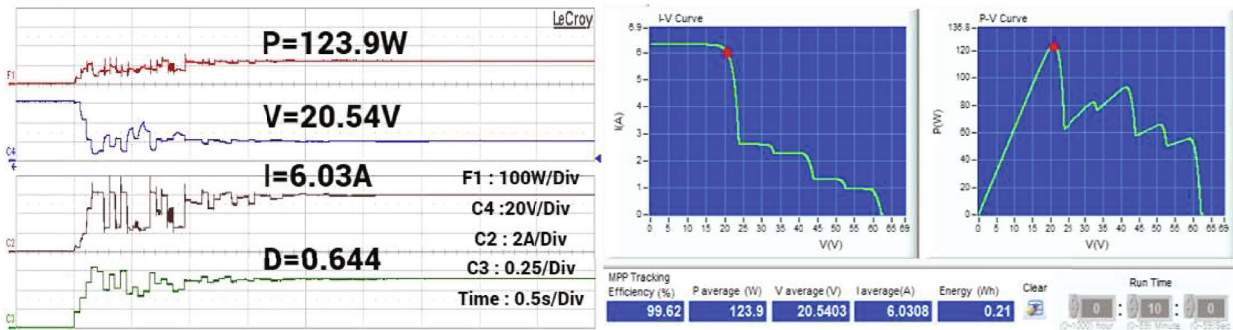FIGURE 31: GWO resulting curves along experimental trial PSC3.

FIGURE 32: GWO resulting curves along experimental trial PSC4.
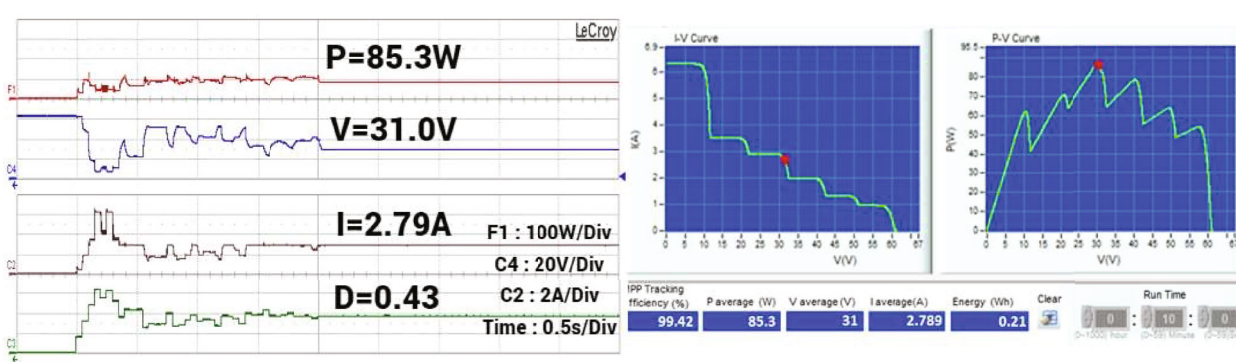

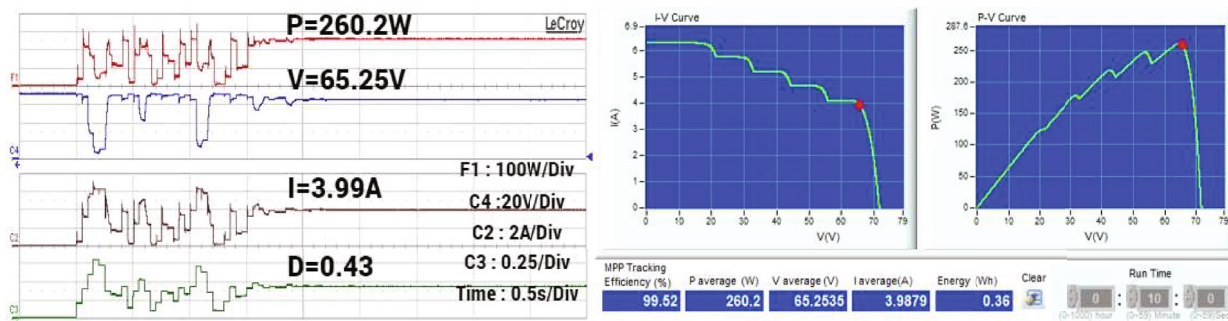FIGURE 33: GWO resulting curves along experimental trial PSC5.

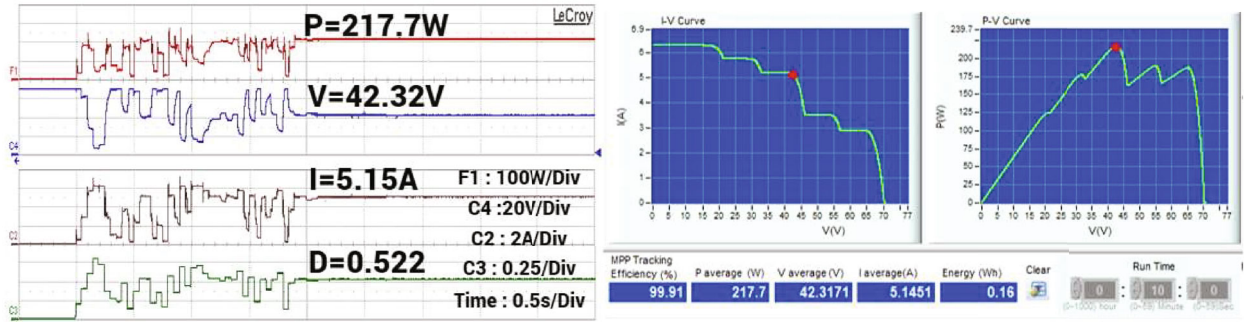FIGURE 34: SMA resulting curves along experimental trial PSC1.

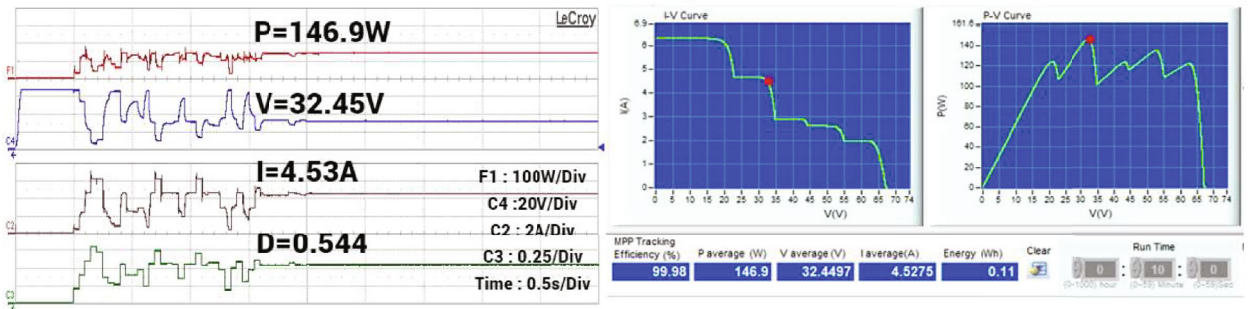Figure 35: SMA resulting curves along experimental trial PSC2.

Figure 36: SMA resulting curves along experimental trial PSC3.
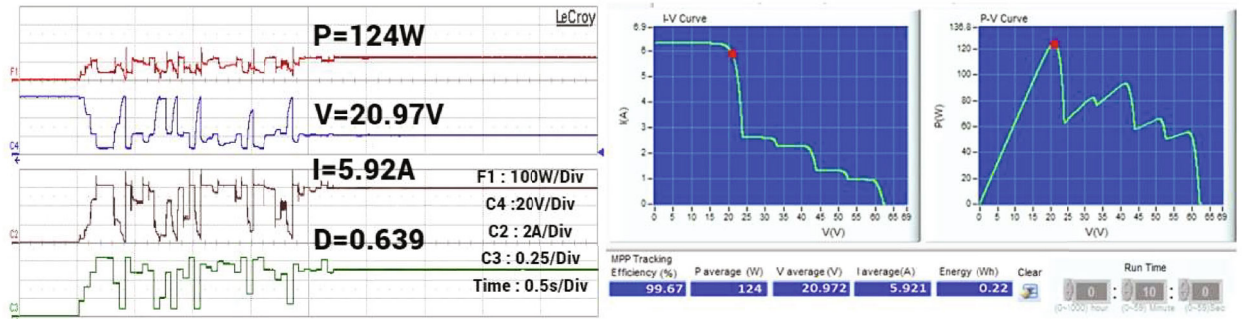

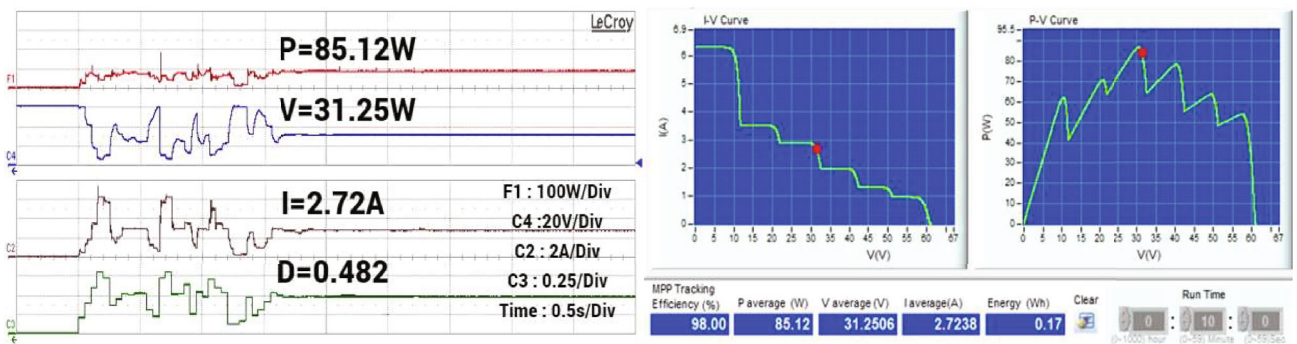Figure 37: SMA resulting curves along experimental trial PSC4.

Figure 38: SMA resulting curves along experimental trial PSC5.

TABLE 3: Reported results of the considered algorithms along the experimental trials.

		HSMA	GWO	PSO	SMA
PSC1	Efficiency (%)	99.92	99.42	99.91	99.52
	Convergence time (s)	0.8	2.7	2.7	2.1
PSC2	Efficiency (%)	99.80	99.56	99.05	99.91
	Convergence time (s)	0.95	2.0	1.75	2.1
PSC3	Efficiency (%)	99.74	99.81	99.42	99.98
	Convergence time (s)	0.6	2.2	1.75	2.0
PSC4	Efficiency (%)	99.95	99.62	99.46	99.67
	Convergence time (s)	0.8	2.0	1.6	2.2
PSC5	Efficiency (%)	99.97	99.42	98.69	98.0
	Convergence time (s)	1.2	2.0	1.6	2.2
Average efficiency (%)		99.876	99.566	99.306	99.416
Average convergence time (s)		0.87	2.18	1.88	2.08

TABLE 4: Overall comparison between the HSMA optimizer and other MPPT techniques.

MPPT algorithm	Tracking speed	Efficiency	Probability of LMPP stagnation under PSC	Fluctuations around the operating point	Fluctuations during the tracking phase	Computational complexity	Number of tuneable parameters
HSMA	Moderate	High	Low	Low	Low	Moderate	1 (convergence factor c)
SMA	Slow	High	Moderate	Low	High	Moderate	2 (convergence factors a, b)
PSO	Slow	High	Moderate	Low	High	Moderate	3 (C_1, C_2, ω)
GWO	Slow	High	Moderate	Low	High	Moderate	1 (convergence factor a)
P&O	Fast	Low	High	High	Very Low	Low	1 (duty cycle perturbation)

Table 3 indicate that the HSMA optimizer comes at the first rank in both average tracking time and average efficiency with the least amount of perturbations.

7. Overall Comparison

The various phases of the HSMA optimizer can be summarized into five distinct sections: power evaluations, sorting, weight calculation, duty cycle update, and memory saving. The computational complexity can then be derived as follows:

$$O(\text{HSMA}) = O(T \times \text{power evaluation}) + O(T \times \text{sorting})$$
$$+ O(T \times \text{weight computation})$$
$$+ O(T \times \text{duty cycle update}),$$

$$(19)$$

where T denotes the number of iterations. Since the previous processes depend on the number of generated solutions N, the computational complexity can be further computed as follows:

$$O(\text{HSMA}) = O(T \times N) + O(T \times N) + O(T \times N \log N)$$
$$+ O(T \times N) = O(T \times N \times (3 + \log N)).$$

$$(20)$$

It has to be highlighted that the main operations of the HSMA optimizer are similar to those in most metaheuristic algorithms. The process starts by generating an initial set of candidate solutions, and then in each iteration, the solutions are updated by the framework equations of the algorithm and evaluated by the defined fitness function. After completing the evaluation process, the best solution or a portion of the best solutions is saved for use in the next iterations.

In order to present a comprehensive assessment of the algorithm overall performance compared to other MPPT techniques, a comparative table that covers the major indices is constructed is given in Table 4. The perturb and observe algorithm (P&O) has been added so that it helps as a reference in the comparison given its minimal computational complexity and rapid tracking speed capabilities.

8. Conclusion

The focal interest of this work was to design an efficient and reliable MPPT algorithm that can handle various partial shading conditions. It was noted from many reported techniques that the validation was carried out on nonuniform irradiance patterns having only few peaks with a global peak that is not hard to detect. In essence, most of the existing techniques are built in such a way they drive the duty ratios rapidly to the spotted optimum region without traversing other potential zones. In light of that, a new performant hyperbolic slime mould algorithm is designed to tackle this issue. The designed optimizer incorporates the hyperbolic tangent function as a way to reduce large distances and hence minify power losses. To foster its global search ability, the algorithm stores the best two solutions that belong to distinct regions of the search space and inspect their neighborhood during the first two iterations. This mechanism of scanning the best two power peak regions allows the algorithm to avoid both redundant exploration and local peak stagnation. A local search operation around the recognized optimum region then takes place along the remaining optimization stages with a rapid convergence trend. To testify its global performance, it was examined through simulation trials of challenging partial shading conditions and compared to the PSO, GWO, and SMA optimizers. Concisely, the HSMA was the winner in all aspects providing higher efficiency, shorter convergence duration, and fewer fluctuations. Moreover, it was shown that the algorithm has an effectual local peak avoidance when exposed to complicated partial shading patterns in which its contenders got rapidly stagnated into the nearest local peak. This benefit is credited to the region inspection mechanism applied to the algorithm and by which the best two optimal zones are effectually exploited before deciding which of which the global best region is. The experimental validation through the DSpace microcontroller and a PV emulator supported the simulation outcomes and proved the algorithm performance, endorsing the HSMA optimizer as an efficient, fast, and reliable MPPT algorithm. Because during uniform irradiance conditions (UICs) the PV characteristic curves are unimodal with a unique peak, global search is unnecessary since it entails a larger tracking time than that of a local search. Given its metaheuristic nature, the designed optimizer behaves the same way during partial shading conditions and uniform irradiance conditions. Therefore, a detection method to distinguish between PSCs and UICs would be highly beneficial to assist the algorithm in deciding whether to perform a global search or a local search process. If a UIC is detected, the algorithm will be confined within the optimum region with a local search operation avoiding traversing the whole PV curve and substantially reducing the tracking time.

Nomenclature

ABC: Artificial bee colony
ACO: Ant colony optimization
DE: Differential evolution
DDM: Double-diode model
FPA: Flower pollination algorithm
GWO: Grey wolf optimizer
HSMA: Hyperbolic slime mould algorithm
InC: Incremental conductance algorithm
MPP: Maximum power point
MPPT: Maximum power point tracking
NM: Nelder-Mead technique
SDM: Single-diode model
SO: Snake optimizer
SSA: Salp swarm algorithm
SMA: Slime mould algorithm
P&O: Perturb and observe algorithm
PS: Partial shading
PSC: Partial shading condition
PSO: Particle swarm optimization
PV: Photovoltaic
UIC: Uniform irradiance conditions
WOA: Whale optimization algorithm
I_{PV}:   Output PV current
I_{ph}:   Photocurrent
I_o: Reverse saturation current
a: Diode ideality factor
R_s: Series resistance
R_{sh}:   Shunt resistance
V_{PV}:   Output PV voltage
P_{PV}:   PV power.

Data Availability

The data used to support the findings of this study are included within the article.

Conflicts of Interest

The authors declare that there is no conflict of interest. The authors declare that they have no known competing financial interests or personal relationships that could have appeared to influence the work reported in this paper.

Acknowledgments

References

[1] M. A. Elgendy, B. Zahawi, and D. J. Atkinson, "Assessment of perturb and observe MPPT algorithm implementation techniques for PV pumping applications," *IEEE Transactions on Sustainable Energy*, vol. 3, no. 1, pp. 21–33, 2011.

[2] D. Sera, L. Mathe, T. Kerekes, S. V. Spataru, and R. Teodorescu, "On the perturb-and-observe and incremental conductance MPPT methods for PV systems," *IEEE Journal of Photovoltaics*, vol. 3, no. 3, pp. 1070–1078, 2013.

[3] F. Yahiaoui, F. Chabour, O. Guenounou et al., "Experimental validation and intelligent control of a stand-alone solar energy conversion system using dSPACE platform," *Frontiers in Energy Research*, vol. 10, article 971384, 2022.

[4] S. Motahhir, A. El Hammoumi, and A. El Ghzizal, "The most used MPPT algorithms: review and the suitable low-cost embedded board for each algorithm," *Journal of Cleaner Production*, vol. 246, article 118983, 2020.

[5] A. F. Mirza, M. Mansoor, and Q. Ling, "A novel MPPT technique based on Henry gas solubility optimization," *Energy Conversion and Management*, vol. 225, article 113409, 2020.

[6] I. Pervez, I. Shams, S. Mekhilef, A. Sarwar, M. Tariq, and B. Alamri, "Most valuable player algorithm based maximum power point tracking for a partially shaded PV generation system," *IEEE Transactions on Sustainable Energy*, vol. 12, no. 4, pp. 1876–1890, 2021.

[7] R. Ahmad, A. F. Murtaza, and H. A. Sher, "Power tracking techniques for efficient operation of photovoltaic array in solar applications–a review," *Renewable and Sustainable Energy Reviews*, vol. 101, pp. 82–102, 2019.

[8] K. Ishaque, Z. Salam, M. Amjad, and S. Mekhilef, "An improved particle swarm optimization (PSO)–based MPPT for PV with reduced steady-state oscillation," *IEEE Transactions on Power Electronics*, vol. 27, no. 8, pp. 3627–3638, 2012.

[9] Y. H. Liu, S. C. Huang, J. W. Huang, and W. C. Liang, "A particle swarm optimization-based maximum power point tracking algorithm for PV systems operating under partially shaded conditions," *IEEE Transactions on Energy Conversion*, vol. 27, no. 4, pp. 1027–1035, 2012.

[10] S. K. Gopalakrishnan, S. Kinattingal, S. P. Simon, and K. Ark Kumar, "Enhanced energy harvesting from shaded PV systems using an improved particle swarm optimisation," *IET Renewable Power Generation*, vol. 14, no. 9, pp. 1471–1480, 2020.

[11] S. Mohanty, B. Subudhi, and P. K. Ray, "A new MPPT design using grey wolf optimization technique for photovoltaic system under partial shading conditions," *IEEE Transactions on Sustainable Energy*, vol. 7, no. 1, pp. 181–188, 2016.

[12] A. M. Eltamaly and H. M. H. Farh, "Dynamic global maximum power point tracking of the PV systems under variant partial shading using hybrid GWO-FLC," *Solar Energy*, vol. 177, pp. 306–316, 2019.

[13] A. F. Mirza, M. Mansoor, Q. Ling, B. Yin, and M. Y. Javed, "A salp-swarm optimization based MPPT technique for harvesting maximum energy from PV systems under partial shading conditions," *Energy Conversion and Management*, vol. 209, article 112625, 2020.

[14] M. N. I. Jamaludin, M. F. N. Tajuddin, J. Ahmed et al., "An effective salp swarm based MPPT for photovoltaic systems under dynamic and partial shading conditions," *IEEE Access*, vol. 9, pp. 34570–34589, 2021.

[15] K. Sundareswaran, P. Sankar, P. S. R. Nayak, S. P. Simon, and S. Palani, "Enhanced energy output from a PV system under partial shaded conditions through artificial bee colony," *IEEE Transactions on Sustainable Energy*, vol. 6, no. 1, pp. 198–209, 2015.

[16] S. K. Sahoo, M. Balamurugan, S. Anurag, R. Kumar, and V. Priya, "Maximum power point tracking for PV panels using ant colony optimization," in *2017 Innovations in Power and Advanced Computing Technologies (i-PACT)*, pp. 1–4, Vellore, India, April 2017.

[17] A. A. Z. Diab and H. Rezk, "Global MPPT based on flower pollination and differential evolution algorithms to mitigate partial shading in building integrated PV system," *Solar Energy*, vol. 157, pp. 171–186, 2017.

[18] H. Chaieb and A. Sakly, "A novel MPPT method for photovoltaic application under partial shaded conditions," *Solar Energy*, vol. 159, pp. 291–299, 2018.

[19] G. Dileep and S. N. Singh, "An improved particle swarm optimization based maximum power point tracking algorithm for PV system operating under partial shading conditions," *Solar Energy*, vol. 158, pp. 1006–1015, 2017.

[20] A. Refaat, A. E. Khalifa, M. M. Elsakka, Y. Elhenawy, A. Kalas, and M. H. Elfar, "A novel metaheuristic MPPT technique based on enhanced autonomous group particle swarm optimization algorithm to track the GMPP under partial shading conditions-experimental validation," *Energy Conversion and Management*, vol. 287, article 117124, 2023.

[21] H. Li, D. Yang, W. Su, J. Lü, and X. Yu, "An overall distribution particle swarm optimization MPPT algorithm for photovoltaic system under partial shading," *IEEE Transactions on Industrial Electronics*, vol. 66, no. 1, pp. 265–275, 2019.

[22] S. Javed and K. Ishaque, "A comprehensive analyses with new findings of different PSO variants for MPPT problem under partial shading," *Ain Shams Engineering Journal*, vol. 13, no. 5, article 101680, 2022.

[23] L. Gong, G. Hou, and C. Huang, "A two-stage MPPT controller for PV system based on the improved artificial bee colony and simultaneous heat transfer search algorithm," *ISA Transactions*, vol. 132, pp. 428–443, 2023.

[24] A. Moghassemi, S. Ebrahimi, S. Padmanaban, M. Mitolo, and J. B. Holm-Nielsen, "Two fast metaheuristic-based MPPT techniques for partially shaded photovoltaic system," *International Journal of Electrical Power & Energy Systems*, vol. 137, article 107567, 2022.

[25] K. T. Swetha, V. Reddy, and A. Robinson, "An innovative grey wolf optimizer with Nelder–Mead search method based MPPT technique for fast convergence under partial shading conditions," *Sustainable Energy Technologies and Assessments*, vol. 59, article 103412, 2023.

[26] K. K. Mohammed and S. Mekhilef, "Improved snake optimizer algorithm-based GMPPT with a fast response to the load variations under different weather conditions for PV systems," *IEEE Transactions on Industrial Electronics.*, pp. 1–11, 2023.

[27] A. M. Eltamaly, M. S. Al-Saud, and A. G. Abokhalil, "A novel scanning bat algorithm strategy for maximum power point tracker of partially shaded photovoltaic energy systems," *Ain Shams Engineering Journal*, vol. 11, no. 4, pp. 1093–1103, 2020.

[28] C. Charin, D. Ishak, M. A. A. M. Zainuri, B. Ismail, and M. K. M. Jamil, "A hybrid of bio-inspired algorithm based on Levy flight and particle swarm optimizations for photovoltaic system under partial shading conditions," *Solar Energy*, vol. 217, pp. 1–14, 2021.

[29] M. Alshareef, Z. Lin, M. Ma, and W. Cao, "Accelerated particle swarm optimization for photovoltaic maximum power point tracking under partial shading conditions," *Energies*, vol. 12, no. 4, p. 623, 2019.

[30] K. Yadav, B. Kumar, J. M. Guerrero, and A. Lashab, "A hybrid genetic algorithm and grey wolf optimizer technique for faster global peak detection in PV system under partial shading," *Sustainable Computing: Informatics and Systems*, vol. 35, article 100770, 2022.

[31] D. Fares, M. Fathi, I. Shams, and S. Mekhilef, "A novel global MPPT technique based on squirrel search algorithm for PV module under partial shading conditions," *Energy Conversion and Management*, vol. 230, article 113773, 2021.

[32] Y. P. Huang, M. Y. Huang, and C. E. Ye, "A fusion firefly algorithm with simplified propagation for photovoltaic MPPT under partial shading conditions," *IEEE Transactions on Sustainable Energy*, vol. 11, no. 4, pp. 2641–2652, 2020.

[33] K. Hu, S. Cao, W. Li, and F. Zhu, "An improved particle swarm optimization algorithm suitable for photovoltaic power tracking under partial shading conditions," *IEEE Access*, vol. 7, pp. 143217–143232, 2019.

[34] S. Li, H. Chen, M. Wang, A. A. Heidari, and S. Mirjalili, "Slime mould algorithm: a new method for stochastic optimization," *Future Generation Computer Systems*, vol. 111, pp. 300–323, 2020.

[35] H. Belmadani, A. Kheldoun, R. Bradai, S. Mekhilef, and M. D. Siddique, "A twofold hunting trip African vultures algorithm for the optimal extraction of photovoltaic generator model parameters," *Energy Sources, Part A: Recovery, Utilization, and Environmental Effects*, vol. 44, no. 3, pp. 7001–7030, 2022.

[36] M. Miyatake, M. Veerachary, F. Toriumi, N. Fujii, and H. Ko, "Maximum power point tracking of multiple photovoltaic arrays: a PSO approach," *IEEE Transactions on Aerospace and Electronic Systems*, vol. 47, no. 1, pp. 367–380, 2011.